HHS Public Access

Author manuscript

Cell. Author manuscript; available in PMC 2024 June 22.

Published in final edited form as:

Cell. 2023 June 22; 186(13): 2802–2822.e22. doi:10.1016/j.cell.2023.04.031.

C5a-licensed phagocytes drive sterilizing immunity during systemic fungal infection

Jigar V. Desai[1,#], **Dhaneshwar Kumar**[2,3], **Tilo Freiwald**[2,@], **Daniel Chauss**[2], **Melissa D. Johnson**[4], **Michael S. Abers**[1], **Julie Steinbrink**[5], **John R. Perfect**[5], **Barbara Alexander**[5], **Vasiliki Matzaraki**[6], **Brendan D. Snarr**[1], **Marissa A. Zarakas**[1], **Vasileios Oikonomou**[1], **Lakmali M. Silva**[7], **Raju Shivarathri**[8], **Emily Beltran**[9], **Luciana Negro Demontel**[9], **Luopin Wang**[3], **Jean K. Lim**[10], **Dylan Launder**[11], **Heather R. Conti**[11], **Muthulekha Swamydas**[1], **Micah T. McClain**[5], **Niki M. Moutsopoulos**[7], **Majid Kazemian**[3], **Mihai G. Netea**[12], **Vinod Kumar**[6,12], **Jörg Köhl**[13], **Claudia Kemper**[9], **Behdad Afzali**[2], **Michail S. Lionakis**[1,§,*]

[1]Fungal Pathogenesis Section, Laboratory of Clinical Immunology & Microbiology, National Institute of Allergy & Infectious Diseases, NIH, Bethesda, USA

[2]Immunoregulation Section, Kidney Diseases Branch, National Institute of Diabetes and Digestive and Kidney Diseases, NIH, Bethesda, USA

[3]Departments of Biochemistry and Computer Science, Purdue University, West Lafayette, USA

[4]Duke Clinical Research Institute, Durham, USA

[5]Department of Medicine, Division of Infectious Diseases, Duke University, Durham, USA

[6]University of Groningen, Department of Genetics, Groningen, Netherlands

[7]Oral Immunity and Infection Section, National Institute of Dental and Craniofacial Research, NIH, Bethesda, USA.

[8]Center for Discovery & Innovation, Hackensack Meridian *Health*, Nutley, USA

[9]Complement and Inflammation Research Section, National Heart Lung and Blood Institute, NIH, Bethesda, USA

[*] lionakism@mail.nih.gov .

[#]Current affiliation: Center for Discovery & Innovation, Hackensack Meridian *Health*, USA

[@]Current affiliation: University Medical Center Hamburg-Eppendorf, Germany

[§]Lead contact

Author contributions

J.V.D. and M.S.L designed and analyzed experiments; J.V.D. performed experiments; D.K., T.F, L.W., D.C., and B.A. analyzed RNA-seq datasets; B.A. and M.K. analyzed eQTL data; M.D.J., M.S.A., J.S., M.T.M. and J.P. analyzed patient outcomes; V.M., M.G.N., and V.K. performed SNP genotyping; V.O., M.A.Z., R.S., B.D.S., L.M.S. and M.S. performed immunoblot, neutrophil functional, and NETosis analyses; N.M. supervised NETosis analyses; B.D.S., E.B., and L.N.D. performed *Lyz2-Cre/C3*$^{fl/fl}$ mouse experiments; K.H. and J.L. performed Luminex-based assays; D.L. and H.C. performed oral candidiasis experiments; J.K. provided C5ar1-reporter and conditional knockout mice; C.K. provided C5-reporter and C5- and C3-conditional knockout mice; J.V.D. and M.S.L. wrote the paper; M.S.L. conceived and supervised the project.

Declaration of interests

The authors declare no conflicts of interest.

[10]Department of Microbiology, Icahn School of Medicine at Mount Sinai, New York, USA

[11]Department of Biological Sciences, University of Toledo, Toledo, USA

[12]Department of Internal Medicine and Radboud Center for Infectious Diseases, Radboud University, Nijmegen, Netherlands

[13]Institute for Systemic Inflammation Research, University of Lübeck, Lübeck, Germany

Summary

Systemic candidiasis is a common, high-mortality, nosocomial fungal infection. Unexpectedly, it has emerged as a complication of anti-complement C5-targeted monoclonal antibody treatment, indicating a critical niche for C5 in antifungal immunity. We identified transcription of complement system genes as the top biological pathway induced in candidemic patients and as predictive of candidemia. Mechanistically, C5a-C5aR1 promoted fungal clearance and host survival in a mouse model of systemic candidiasis by stimulating phagocyte effector function and ERK/AKT-dependent survival in infected tissues. *C5ar1* ablation rewired macrophage metabolism downstream of mTOR, promoting their apoptosis and enhancing mortality through kidney injury. Besides hepatocyte-derived C5, local C5 produced intrinsically by phagocytes provided a key substrate for antifungal protection. Lower serum C5a concentrations or a *C5* polymorphism that decreases leukocyte *C5* expression correlated independently with poor patient outcomes. Thus, local, phagocyte-derived C5 production licenses phagocyte antimicrobial function and confers innate protection during systemic fungal infection.

In Brief

Locally-produced complement component C5 is a critical mediator of anti-fungal defense in infected tissues, and this finding explains the susceptibility of patients to systemic *Candida* infection after C5 inhibition therapy.

Graphical Abstract

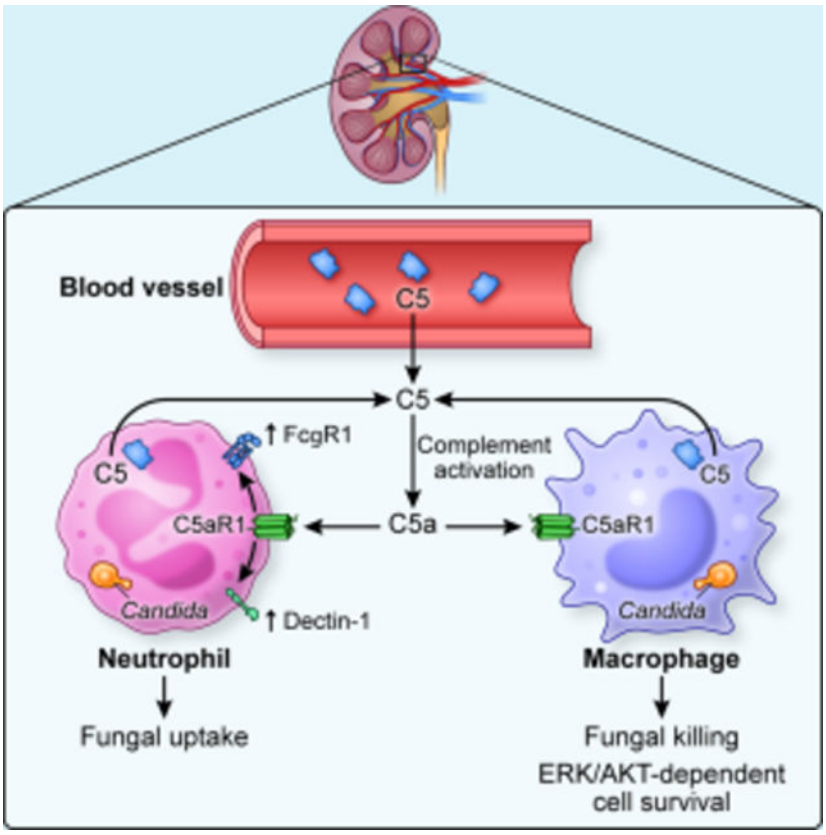

Keywords

Complement; C5; C5aR1; *Candida* ; candidemia; candidiasis; kidney

Introduction

Systemic candidiasis is a public health threat causing >700,000 cases/year with high mortality despite therapy[1,2]. It recently emerged as an unexpected complication of complement C5-targeted monoclonal antibody treatment[3–5], indicating that complement activation orchestrates protective antifungal responses. Phagocyte-dependent responses are critical for defense during systemic candidiasis[6,7]. Improving our understanding of these responses could enable personalized risk stratification, immunotherapy, and vaccination strategies in at-risk patients and improve their outcomes.

The complement system is crucial for bacterial clearance[8]. Complement activation converges on C5 cleavage into C5a and C5b. C5a is a potent chemoattractant and C5b forms the multiprotein membrane attack complex for bacterial lysis[9]. Unsurprisingly, inherited *C5* deficiency causes life-threatening invasive infections by encapsulated bacteria (e.g., meningococcus, pneumococcus)[10]. Conversely, dysregulated complement activation exacerbates inflammation and tissue injury as seen in patients with paroxysmal nocturnal hemoglobinuria or atypical hemolytic syndrome[9,11,12], who are effectively treated with the FDA-approved anti-C5 antibody, eculizumab[3,13]. As with inherited *C5* deficiency,

eculizumab predisposes to invasive encapsulated bacterial infections. Unexpectedly, post-marketing pharmacovigilance revealed that eculizumab also increases the risk of life-threatening systemic fungal infections[3,4], leading the FDA to update its package insert to warn against this risk[5]. These observations suggest a critical yet unexpected role for C5 in human antifungal defense mechanisms.

Although complement is traditionally considered hepatocyte-derived and plasma-operative, complement components are also expressed and biologically-active intracellularly. C5, for example, is expressed by lymphocytes and phagocytes, and acts as a substrate for C5a generation locally within tissues[8,14]. Although C5 produced by $CD4^+$ T cells and monocytes/macrophages supports IFN-γ and IL-1β secretion, respectively[15,16], whether locally-produced C5 contributes to antimicrobial defense is unknown.

Here, we studied complement-dependent immune responses during systemic candidiasis in patients and in a mouse model of the infection. In patients, we found that transcription of complement genes is the top biological pathway induced in candidemia and is predictive of the disease. We also found that suboptimal complement activation due to either decreased serum C5a concentrations or a *C5* SNP is an independent risk factor for poor clinical outcomes. In mice, we show that C5a-C5aR1 signaling in phagocytes is essential for immunological fitness to *Candida* challenge, mediating phagocyte survival, optimal cellular metabolism, and effector function, thereby promoting fungal clearance and host survival. We demonstrate that this mechanism relies on locally-produced C5 within *Candida*-infected tissue by phagocytes, highlighting it as a critical anti-microbial mediator during systemic fungal infection and explaining the susceptibility of eculizumab-treated patients to fungal disease.

Results

Induced transcription of complement genes in human whole blood predicts candidemia

To investigate the role of complement in defense against systemic candidiasis, we sourced bulk RNA-seq data from whole blood of 47 candidemic patients and 29 healthy controls (GSE176262)[17]. We compared the transcriptomes of patients to healthy controls using gene-set enrichment analysis (GSEA)[18] and found 125 *Hallmark* and *Canonical* pathways curated by the Molecular Signatures Database (MSigDB)[19] to be enriched in the patient transcriptomes. Four of these were annotated as complement pathways (Table S1A). Ordering of enriched pathways by normalized enrichment score showed that complement pathways were among the most enriched and that complement was, in fact, *the* topmost enriched of all pathways (Figure 1A). To contextualize these observations, we also analyzed bulk RNA-seq data from whole blood of patients hospitalized with bacterial infections (n=45), viral infections (n=59), or non-infectious systemic inflammatory response syndrome (SIRS; n=17), i.e., those with sepsis features without identifiable infection. Although complement genes were also induced under these conditions, their induction especially during bacterial infection or SIRS was not as dramatic as in candidemic patients (Figure 1B). To identify complement genes induced in candidemic patients, we combined the leading edges of the enriched complement pathways to generate a complement “module” (Table S1B). This module was noteworthy for genes of the classical pathway of complement

activation, including *C1QA*, *C1QB*, *C1QC*, *C4A*, *C4B,* and several immunoglobulin genes (Table S1B; Figure 1C). Expression of this module was significantly induced in candidemic patients relative to healthy controls (Figure 1D), and was a strong predictive biomarker for distinguishing candidemic patients from healthy controls with an area under the receiver operating characteristic (ROC) curve of 0.94 (Figure 1E). Expression of this module appeared more specific to candidemia, as it performed less well at distinguishing healthy controls from other types of infection or inflammation (AUC 0.76–0.79; Figure 1E). To further contextualize this module's performance, we performed ROC analysis of all 2545 pathways curated by MSigDB and ranked their predictive power. The complement module was among the very top-ranked pathways as a predictive biomarker for candidemia, being within the top 2% of all pathways (Figure 1F; Table S1C).

To independently validate this module, we sourced bulk RNA-seq data from peripheral blood mononuclear cells (PBMCs) of healthy donors challenged *ex vivo* with *C. albicans* (GSE162746)[20]. We found significant induction of the same complement module upon PBMC exposure to *Candida,* but not mold fungi (Figure 1G). Thus, the observed activation of complement gene transcription in whole blood leukocytes of candidemic patients likely represents an intrinsic response to *Candida* and does not appear to be primarily related to severe acute illness or sepsis in these patients. Collectively, these data show that activation of complement transcription in whole blood leukocytes is the top biological pathway induced in candidemic patients and one of the top predictive biomarkers of candidemia.

C5a-C5aR1 signaling promotes fungal clearance and host survival in murine systemic candidiasis

Since the anti-C5 antibody eculizumab is implicated in the development of systemic candidiasis in humans, we postulated that C5 levels might be associated with candidiasis. We examined the expression of *C5* mRNA in bulk RNA-seq data from whole blood of candidemic patients and healthy controls (GSE176262)[17]. *C5* expression was significantly greater in candidemic patients (Figure 1H). Moreover, C5 protein levels were induced in monocytes from healthy donors upon stimulation with *C. albicans,* but not *Aspergillus, ex vivo* (Figures 1I–J). Collectively, these data show activation of *C5* transcription in whole blood leukocytes of candidemic patients and *Candida*-mediated induction of C5 protein in human monocytes.

To understand how C5a-induced cell activation protects against systemic candidiasis, we used an established mouse model, where *C. albicans* is injected intravenously and spreads to several tissues, with kidneys being the primary target[21,22]. We suspected an *in vivo* protective function for C5 because C5-deficient inbred A/J and DBA/2 mouse strains are susceptible to death from systemic candidiasis in this model[23–26]. However, because these strains demonstrate additional immunological defects[27,28], the immunological mechanisms for *Candida* susceptibility were not previously established.

We first analyzed bulk RNA-seq data from wild-type (WT) mouse kidneys at steady-state and at different timepoints post-systemic candidiasis using GSEA (GSE56092)[29]. Complement pathway genes were enriched in transcriptomes post-infection relative to the uninfected state, and ranked among the very top *Hallmark* and *Canonical* MSigDB pathways

(Figure 2A; Table S2). Notably, the leading edge genes of induced complement pathways contained *C5* and *C5ar1,* one of the two cognate C5a receptors (Figures 2B–C)[14]. We confirmed increased expression of *C5* and *C5ar1,* but not *C5ar2*, the other cognate C5a receptor[14], in *Candida*-infected kidneys by RT-qPCR (Figure S1A). Moreover, we observed significantly increased serum C5a concentrations following systemic candidiasis compared to the steady-state (Figure S1B), indicative of systemic complement activation *in vivo*.

To test the protective role of C5a in candidemic mice, we administered recombinant C5a to *Candida*-infected WT animals and observed significantly improved survival compared to vehicle (Figure 2D). Since C5a can signal through C5aR1 and C5aR2, we infected *C5ar1*$^{-/-}$ and *C5ar2*$^{-/-}$ mice. *C5ar1*$^{-/-}$ mice were highly-susceptible and exhibited universal mortality by day 6 post-infection, whereas 60% of *C5ar1*$^{+/+}$ mice remained alive 28 days post-infection (Figure 2E). *C5ar1*$^{-/-}$ mice had significantly greater fungal burden in several organs throughout the infection and as early as 2 hours post-infection in the kidney (Figures 2F; S1C). Impaired control of renal fungal proliferation in *C5ar1*$^{-/-}$ mice was accompanied by reduced kidney function (Figure 2G). Histological examination of *C5ar1*$^{-/-}$ kidneys showed markedly increased fungal invasion, inflammatory lesions, and tissue damage (Figure 2H). By contrast, *C5ar2*$^{-/-}$ mice had similar survival, tissue fungal burden, kidney function, and histological appearances compared to WT mice (Figures S1D–G). Furthermore, consistent with the segregation of host requirements for controlling systemic versus mucosal candidiasis[30], C5aR1 was dispensable for fungal clearance during oropharyngeal and vulvovaginal candidiasis (Figures S1H–I). Collectively, these data indicate that complement activation is among the cardinal features of murine systemic candidiasis and that protective immunity is dependent on C5a signaling downstream of C5aR1 to prevent mortality.

C5aR1 signaling specifically in phagocytes protects against systemic candidiasis

C5aR1 is expressed on hematopoietic and non-hematopoietic cells, including renal tubular cells and pericytes[31–34]. To assess whether increased susceptibility of *C5ar1*$^{-/-}$ mice during systemic candidiasis is driven by C5aR1 deficiency in the hematopoietic and/or stromal compartments, we generated bone marrow (BM) chimeras. WT mice reconstituted with *C5ar1*$^{-/-}$ BM, but not *C5ar1*$^{-/-}$ mice reconstituted with WT BM, were susceptible to systemic candidiasis and exhibited similar susceptibility as *C5ar1*$^{-/-}$ mice reconstituted with *C5ar1*$^{-/-}$ BM (Figures S2A–D). Therefore, C5aR1 within hematopoietic cells protects during systemic candidiasis.

Neutrophils, monocytes, macrophages, and CD11b^{+} dendritic cells (DCs) are indispensable for defense in the model of systemic candidiasis[35]. To delineate the cells that are dependent on C5aR1 signaling during systemic candidiasis, we examined C5aR1 expression on leukocyte subsets (gating strategy: Figure S2E) in *Candida*-infected kidneys using *GFP-C5ar1*$^{fl/fl}$ reporter mice[31]. C5aR1 was highly-expressed on neutrophils and macrophages, whereas monocytes displayed intermediate C5aR1 expresssion, and DCs and lymphocytes expressed C5aR1 at low levels (Figures S2F–G). To define the differential contributions of C5aR1-expressing phagocytes in protection during systemic candidiasis, we generated mice with conditional C5aR1 ablation in neutrophils, monocytes/macrophages or all

phagocytes[36–38]. *Lyz2-Cre/C5ar1*$^{fl/fl}$ mice were highly susceptible to systemic candidiasis and recapitulated the phenotype of *C5ar1*$^{-/-}$ mice (Figures 2I–J; S2H). Mice with specific *C5ar1* ablation in neutrophils (*S100a8-Cre/C5ar1*$^{fl/fl}$) or monocytes/macrophages (*Cx3cr1-Cre/C5ar1*$^{fl/fl}$) also increased susceptibility to systemic candidiasis (Figures 2I–J; S2H). Thus, C5a-C5aR1 signaling on both polymorphonuclear and mononuclear phagocytes protects from systemic candidiasis.

C5aR1 is dispensable for phagocyte recruitment into the kidney

We next aimed to examine whether C5aR1 deficiency impairs phagocytes quantitatively and/or qualitatively to enhance susceptibility to systemic candidiasis. C5a is a potent chemoattractant and C5aR1 drives neutrophil and monocyte recruitment in several infectious and non-infectious settings[39–45]. We reasoned that C5aR1 protects during systemic candidiasis by mediating phagocyte recruitment to the *Candida*-infected kidneys. We quantified the temporal accumulation of phagocyte subsets in *C5ar1*$^{+/+}$ and *C5ar1*$^{-/-}$ kidneys[46,47], and observed, contrary to expectations, greater accumulation of neutrophils and monocytes in the *C5ar1*$^{-/-}$ *Candida*-infected kidneys, whereas DC accumulation was unchanged relative to WT mice (Figures 3A, S3A–C). In agreement, we found increased levels of neutrophil-targeted and monocyte-targeted chemokines in infected *C5ar1*$^{-/-}$ kidneys (Figure S3D). Furthermore, the induction of other protective pro-inflammatory mediators in this model, many of which are phagocyte-derived, such as IL-1β, IL-6, GM-CSF, and TNF-α[48–52], was not decreased in *C5ar1*$^{-/-}$ kidneys post-infection (Figure S3E).

Renal accumulation of neutrophils and monocytes is proportional to the local fungal burden in the model of systemic candidiasis[22,46,47]. Because of the markedly increased fungal burden in *C5ar1*$^{-/-}$ relative to WT kidneys (Figure 2F), we generated mixed BM radiation chimeras. We adoptively transferred CD45.1^{+}*C5ar1*$^{+/+}$ and CD45.2^{+}*C5ar1*$^{-/-}$ donor BM cells at a 1:1 ratio into lethally-irradiated CD45.1^{+}*C5ar1*$^{+/+}$ recipient mice, and infected them post-engraftment (Figure S3F). The relative frequency of CD45.1^{+}*C5ar1*$^{+/+}$ and CD45.2^{+}*C5ar1*$^{-/-}$ neutrophils, Ly6C^{hi} monocytes, and Ly6C^{lo} monocytes was similar between infected blood and kidney, indicating that recruitment of *C5ar1*$^{-/-}$ neutrophils and monocytes from the blood into kidneys was not perturbed compared to WT cells (Figure 3B). Collectively, these data show that C5aR1 is dispensable for neutrophil and monocyte recruitment or production of pro-inflammatory mediators in the infected kidney during systemic candidiasis.

C5aR1 is non-redundant for macrophage accumulation and survival and inhibits caspase-dependent apoptosis

In contrast to neutrophils and monocytes, we observed significantly decreased macrophages in infected *C5ar1*$^{-/-}$ kidneys (Figures 3A, S3A). Quantitative deficiency of macrophages impairs fungal clearance and host survival during systemic candidiasis[46,53,54]. Therefore, we examined the mechanisms of decreased macrophage accumulation in *C5ar1*$^{-/-}$ kidneys, which could be explained by decreased (a) monocyte recruitment from the blood into the kidney, and/or (b) macrophage proliferation, and/or (c) macrophage survival. We observed no defect in monocyte recruitment from blood into the infected *C5ar1*$^{-/-}$ kidneys (Figures 3A–B, S3A) and the proportion of proliferating Ki-67^{+} macrophages was similar between

C5ar1$^{+/+}$ and *C5ar1*$^{-/-}$ kidneys (Figure S4A). By contrast, we observed significantly increased Indo-1^{+} or PI^{+} dead macrophages in *C5ar1*$^{-/-}$ relative to WT kidneys (Figures 3C–D). Consequently, the proportion of viable macrophages was significantly greater in WT kidneys (Figures 3D).

Consistent with C5aR1 promoting survival by blocking apoptosis in CD4^{+} T cells[55], the proportion of annexin V^{+}PI^{-} apoptotic renal macrophages was significantly increased in infected *C5ar1*$^{-/-}$ kidneys (Figure 3D). In agreement, renal *C5ar1*$^{-/-}$ macrophages exhibited increased levels of the pro-apoptotic effector molecules Bax and cleaved caspase-3 (Figures 3E–F). To examine whether increased macrophage apoptosis in the absence of C5aR1 is cell-intrinsic or due to the increased renal fungal load of *C5ar1*$^{-/-}$ mice, we generated mixed 1:1 WT:*C5ar1*$^{-/-}$ BM chimeras. We found enhanced apoptosis and cell death, increased expression of pro-apoptotic molecules, and decreased survival of *C5ar1*$^{-/-}$ relative to WT renal macrophages in this setting (Figures 3G–H). In keeping with a cell-intrinsic survival defect of C5aR1-deficient macrophages, we also found increased apoptosis and cell death and decreased survival of *C5ar1*$^{-/-}$ relative to WT BM-derived macrophages upon co-culture with *Candida in vitro* (Figure 3I).

We also examined non-apoptotic mechanisms of cell death as *C. albicans* can induce pyroptosis, necroptosis, and ferroptosis in macrophages[56–59]. Interestingly, *C5ar1*$^{-/-}$ renal macrophages displayed increased cleaved caspase-1 and cleaved gasdermin D, indicative of activated pyroptosis (Figure S4B). WT and *C5ar1*$^{-/-}$ LPS-stimulated BM-derived macrophages exhibited similar levels of cleaved gasdermin D upon *Candida* co-culture *in vitro* (Figure S4C), suggesting that increased pyroptosis of *C5ar1*$^{-/-}$ renal macrophages is likely cell-extrinsic, reflecting local changes in the micro-environment of *C5ar1*$^{-/-}$ infected kidneys. By contrast, we detected similar amounts of phosphorylated Mlkl and Gpx4 as surrogate markers of necroptosis and ferroptosis, respectively, in WT and *C5ar1*$^{-/-}$ renal macrophages (Figure S4D). Collectively, these data show that C5aR1 promotes macrophage accumulation in the infected kidney by promoting their survival, not via affecting their proliferation or monocyte recruitment. The C5aR1-dependent survival benefit is mediated via inhibiting caspase-dependent apoptosis and pyroptosis.

We next aimed to define the C5a-dependent signaling cascades involved in ameliorating macrophage apoptosis and death. We focused on extracellular signal-regulated protein kinase (ERK1/2) and protein kinase B (AKT) as these kinases are activated by C5a-C5aR1 in myeloid cells[60] and were shown to promote human monocyte survival downstream of G protein-coupled receptor engagement[61]. We found increased ERK1/2 and AKT phosphorylation in WT BM-derived macrophages upon C5a treatment, which was synergistically enhanced in the presence of *Candida* (Figure 3J–K). We then assessed the role of these signaling kinases on promoting macrophage survival downstream of C5aR1 activation. C5a treatment decreased apoptosis and cell death and increased survival of WT BM-derived macrophages co-cultured with *Candida in vitro* (Figures 3L–M). This C5a-induced amelioration of macrophage apoptosis was abrogated by pharmacological inhibition of ERK1/2 or AKT signaling (Figures 3L–M). Collectively, these data indicate that C5a promotes C5aR1-mediated macrophage survival via ERK1/2- and AKT-dependent inhibition of apoptosis.

C5aR1 mediates fungal uptake by neutrophils and killing by macrophages

We next explored how C5aR1 deficiency may affect phagocytic antifungal functions. In the WT setting, phagocytes restrict *Candida* proliferation via phagocytosis and intracellular killing of yeast cells and extracellular destruction of filamentous hyphae[30,62], which is the virulent morphogenic fungal state[63]. We first used a fluorescence-based "functional microbial reporter"[64,65] to assess uptake and intracellular killing of *Candida* yeast cells by renal phagocytes *in vivo*[66,67] (Figure S4E). We observed significantly lower yeast cell uptake by *C5ar1*$^{-/-}$ neutrophils, whereas intracellular yeast cell killing was unimpaired (Figure 4A). Congruently, neutrophil reactive oxygen species (ROS) production and neutrophil extracellular trap formation were not decreased in *C5ar1*$^{-/-}$ mice (Figures S4F–G). Kidney monocytes did not exhibit C5aR1-dependent uptake or intracellular killing of yeast cells (Figure 4B). Interestingly, although *C5ar1*$^{-/-}$ renal macrophages appeared to associate normally with yeast cells, they exhibited impaired intracellular yeast cell killing (Figure 4C). We FACS-sorted renal macrophages and independently confirmed the dependence on C5aR1 for macrophage fungal killing *ex vivo* (Figure 4D), whereas no defect was seen in macrophage ROS production (Figure S4H). Therefore, C5aR1 deficiency impairs yeast cell uptake by neutrophils and intracellular non-oxidative killing by macrophages.

To probe neutrophil and macrophage interactions with *Candida in vivo* in real-time, we developed a multicolor intravital microscopy approach. We focused on early phagocyte-*Candida* interactions[46], and found that whereas ~80% of yeast cells were associated with neutrophils in WT kidneys, only ~15% yeast cells were associated with *C5ar1*$^{-/-}$ neutrophils (Figures 4E, F; Movie S1). This observation was not due to differential numbers, sphericity, or velocity of WT and *C5ar1*$^{-/-}$ neutrophils (Figures S4I–J). By contrast, we found no difference in *C. albicans* growth inhibition once the fungus was associated with neutrophils, irrespective of the genotype (Figure 4G). With regard to renal macrophages, their association with *Candida* was similar in WT and *C5ar1*$^{-/-}$ mice (Figures 4F, H). However, whereas fungal-associated WT macrophages universally restricted *C. albicans* growth, fungal-associated *C5ar1*$^{-/-}$ macrophages permitted *C. albicans* growth in 82% of the examined interactions at an average rate of 8 μm/hour (Figures 4G–I; Movie S1). Strikingly, the impairment in fungal uptake by neutrophils and growth restriction by macrophages in *C5ar1*$^{-/-}$ kidneys was collectively associated with a marked inability to restrict fungal filamentation *in vivo*. Indeed, whereas ~80% of examined yeast cells germinated into filamentous hyphae in the *C5ar1*$^{-/-}$ kidney, only ~5% of filamentation occurred in the WT kidney within the first hour post-infection (Figure 4J).

We next examined whether the defects in fungal uptake and killing by *C5ar1*$^{-/-}$ renal neutrophils and macrophages were caused by cell-intrinsic defects or whether they were driven by the local immunological milieu of infected *C5ar1*$^{-/-}$ kidneys. Neutrophils and macrophages harvested from the BM of uninfected *C5ar1*$^{-/-}$ mice exhibited similar defects in fungal uptake and killing, respectively (Figures 4K, S4K). Moreover, C5a treatment enhanced fungal uptake and killing by WT BM neutrophils and macrophages, respectively, *in vitro* (Figure 4L). We then asked whether C5AR1 inhibition impairs the antifungal function of human phagocytes. We treated human blood neutrophils and monocyte-derived

macrophages with the C5AR1 inhibitor, avacopan, which was recently FDA-approved for the treatment of anti-neutrophil cytoplasmic antibody-associated vasculitis[68]. Avacopan decreased fungal uptake and killing by human neutrophils and macrophages, respectively (Figure 4M), indicating that avacopan has the potential to heighten the risk of fungal disease in humans. Collectively, these data show that C5aR1 deficiency causes cell-intrinsic defects in neutrophil fungal uptake and macrophage fungal killing, cumulatively resulting in failure to prevent fungal filamentation *in vivo*.

Since C3a is a major complement effector upstream of C5a, we wondered whether it exerts similar functions to C5a during fungal challenge. As with C5a, C3a was increased in *Candida*-infected mouse sera relative to steady-state (Figure S5A), and administration of recombinant C3a in WT mice improved their survival post-infection (Figure S5B). *C3*$^{-/-}$ mice rapidly died after systemic candidiasis (Figure S5C), confirming prior observations[69], and were resistant to oropharyngeal candidiasis (Figure S1H), thereby phenocopying the susceptibility of *C5ar1*$^{-/-}$ mice (Figures 2E, S1H). We exposed WT BM neutrophils and BM-derived macrophages to *Candida in vitro*, and asked whether C3a modulates their survival and effector functions as C5a did. C3a decreased apoptosis and cell death and increased survival of macrophages (Figures S5D–E), similar to C5a (Figures 3L–M). By contrast, C3a did not directly affect neutrophil fungal uptake or macrophage killing (Figures S5F). Collectively, these data indicate that C3a protects against murine systemic candidiasis and reveal similarities and differences on the mechanistic roles of C3a and C5a in phagocytes.

Phagocytic molecules are decreased in *C5ar1*$^{-/-}$ neutrophils

We next FACS-sorted neutrophils and macrophages from infected *C5ar1*$^{+/+}$ and *C5ar1*$^{-/-}$ kidneys and performed bulk RNA-seq. Principal component analysis separated the transcriptomes of WT and *C5ar1*$^{-/-}$ neutrophils and macrophages along the first two principal components (PCs), approximately by cell-type (PC1) and genotype (PC2), demonstrating clear differences in transcriptional programs in cells lacking C5aR1 (Figure S6A). 1966 transcripts were differentially expressed (>2-fold change in either direction at adjusted $P<0.01$) in *C5ar1*$^{-/-}$ relative to WT neutrophils (Figures S6B–C; Table S3A). We compared the transcriptomes of *C5ar1*$^{+/+}$ and *C5ar1*$^{-/-}$ neutrophils by GSEA for enrichment of the positive regulation of phagocytosis geneset curated by gene ontology (GO:0050766). Genes in this geneset were more highly expressed by WT compared to *C5ar1*$^{-/-}$ neutrophils (Figure S6D). Among the leading edge of genes from this geneset were *Clec7a* and *Fcgr1*, which encode the bona-fide phagocytic receptors Dectin-1 and high-affinity Fc receptor (FcγR1), respectively. Both receptors were more significantly expressed in WT neutrophils (Figure S6D; Table S3A). In agreement, we found decreased protein levels of Dectin-1 and FcγR1 on the surface of *C5ar1*$^{-/-}$ neutrophils harvested from *Candida*-infected kidneys of *C5ar1*$^{-/-}$ and of mixed 1:1 WT:*C5ar1*$^{-/-}$ BM chimeric mice and from uninfected mouse BM (Figure S6E–G) Exposure of WT BM neutrophils to C5a and *Candida* synergistically up-regulated Dectin-1 and FcγR1 expression *in vitro* (Figure S6G). Thus, C5a-C5aR1 promotes neutrophil fungal uptake associated with increased expression of phagocytic receptors.

mTORC1-associated metabolic rewiring is enhanced in *C5ar1*$^{-/-}$ renal macrophages

We next compared the transcriptomes of WT and *C5ar1*$^{-/-}$ macrophages for differentially-enriched biological pathways among the *Hallmark* pathways curated by MSigDB. 915 transcripts were differentially expressed in *C5ar1*$^{-/-}$ relative to WT macrophages (Figure S6B; Table S3B). Transcripts of the *Hallmark apoptosis pathway* were enriched in *C5ar1*$^{-/-}$ macrophages (Figures 5A, S6H; Table S3C), in agreement with their enhanced caspase-dependent apoptotic cell death (Figures 3C–D). Notably, some of the most enriched genesets in *C5ar1*$^{-/-}$ renal macrophages were glycolysis, mTORC1 signaling, and ROS pathway, suggestive of metabolic rewiring (Figures 5A, S6H; Table S3C). Indeed, *C5ar1*$^{-/-}$ renal macrophages had greater expression of phosphorylated ribosomal protein S6, indicative of enhanced mTORC1 activity, increased levels of the glucose transporter Glut1, and increased extracellular acidification rate and oxygen consumption rate by Seahorse extracellular flux analysis compared to WT macrophages (Figures 5B–C).

mTORC1 signaling regulates cellular energetics, including glycolysis, and survival in phagocytes[70]. Pharmacological inhibition of hyperactive mTORC1 rescues macrophages from apoptotic cell death during sterile inflammation[71–73]. Thus, we reasoned that pharmacological inhibition of hyperactive mTORC1 in *C5ar1*$^{-/-}$ mice may ameliorate apoptotic cell death in macrophages and improve the outcome of systemic candidiasis. Indeed, treatment of *C5ar1*$^{-/-}$ mice with the FDA-approved mTOR inhibitor rapamycin decreased p-S6 and Glut1 expression, reduced the proportion of apoptotic and dead cells, and decreased the expression of cleaved caspase-3 and Bax in *C5ar1*$^{-/-}$ renal macrophages (Figures 5D–E), and improved kidney function and survival of *C5ar1*$^{-/-}$ mice (Figures 5F–G). The protective effects of rapamycin on reducing macrophage apoptosis and improving renal function and survival in *C5ar1*$^{-/-}$ mice were also seen following infection with the isogenic rapamycin-resistant *C. albicans* strain *rbp1Δ/Δ*[74], albeit to a lesser degree for mouse survival (Figures 5H–J). Moreover, rapamycin decreased apoptosis and cell death and increased survival of WT and *C5ar1*$^{-/-}$ BM-derived macrophages upon co-culture with the rapamycin-resistant strain *rbp1Δ/Δ in vitro* (Figure 5K), indicative of a direct protective effect of rapamycin on macrophages that is independent of its *in vitro* antifungal activity[74]. Collectively, these data identify enhanced mTORC1 signaling in *C5ar1*$^{-/-}$ renal macrophages as a regulator of apoptosis that can be targeted with therapeutic benefit during systemic candidiasis.

Renal phagocyte-intrinsic, locally-produced C5 is essential for fungal clearance

Hepatocytes are major producers of circulating complement proteins, including C5[75]. To examine the contribution of liver-derived C5 to the protective antifungal response during systemic candidiasis, we infected *Albumin-Cre*^{tg}*/C5*$^{fl/fl}$ mice, which specifically lack C5 in hepatocytes and are consequently plasma C5-deficient. *Albumin-Cre*^{tg}*/C5*$^{fl/fl}$ mice exhibited increased renal fungal proliferation, albeit to a lesser extent than *C5ar1*$^{-/-}$ mice (Figure 2F), increased tissue fungal invasion and kidney injury upon histological examination, and impaired kidney function post-infection (Figures 6A–B). Thus, liver-derived C5 is critical for protection during systemic candidiasis.

Besides hepatocytes, extrahepatic complement production can play significant roles in immune regulation[76]. Myeloid cells can produce C5 locally, providing a source of C5a in tissues, where plasma-derived C5 is absent[8,14,75]. Phagocyte-derived, locally-produced C5 supports IL-1β secretion by monocytes/macrophages and can drive sterile inflammation[15]. However, it is unclear whether local leukocyte-intrinsic C5 generation contributes to antimicrobial defense. We examined this question, as we observed induced *C5* mRNA in whole blood leukocytes of candidemic patients and in *Candida*-infected kidneys and we found that *Candida* up-regulated C5 protein expression in human monocytes (Figures 1H–J, 2B–C, S1A). We studied renal cell subsets for C5 expression at steady-state and post-infection using *YFP-C5*$^{fl/fl}$ reporter mice[15]. Renal phagocytes expressed C5 at steady-state and during systemic candidiasis. C5 was up-regulated at day 1 and/or 3 post-infection over the uninfected state in neutrophils, monocytes, and CD11b^{+} DCs. C5 expression was also noted in renal stromal cells (Figures 6C–D, S6I).

To determine whether phagocyte-specific C5 production contributes to antifungal immunity, we generated *Lyz2-Cre*^{tg}*/C5*$^{fl/fl}$ mice, which exhibited significantly increased mortality and renal fungal burden, and reduced kidney function post-infection (Figure 6E), albeit to a lesser degree than *C5ar1*$^{-/-}$ mice (Figures 2E–F). Moreover, histological examination revealed increased tissue fungal invasion and kidney injury in *Lyz2-Cre/C5*$^{fl/fl}$ mice (Figure 6F). By contrast, phagocyte-specific C3 production was dispensable for fungal control during systemic candidiasis as *Lyz2-Cre/C3*$^{fl/fl}$ mice did not exhibit increased kidney fungal proliferation or tissue invasion or weight loss (Figure S5G–I), indicating that hepatocyte-derived C3 may mediate the C3-dependent protection in this model. Collectively, our findings provide direct evidence that besides liver-derived C5, local C5 production by phagocytes in the fungal-infected kidney is essential to innate antifungal protection.

A *C5* SNP is independently associated with persistent candidemia in patients

To examine whether variations in leukocyte-intrinsic C5 expression may affect candidemic patient outcomes, we sourced data of *cis*-expression quantitative trait loci (*cis*-eQTLs)[77] that influence *C5* expression in human whole blood at steady-state. We found that *C5* SNP rs2269067 (G>C) was within a highly-enriched locus in strong linkage disequilibrium with several of the top-enriched *cis*-eQTLs affecting *C5* expression (Figure 6G). In agreement, PBMCs from individuals harboring the C allele exhibit decreased *C5* mRNA levels[78,79], which we independently confirmed (Figure 6H).

We asked whether the presence of the C allele is associated with poor outcomes in candidemic patients by analyzing a separate patient cohort (n=169) (Table S4). Although there was no association between carrying the C allele and disseminated infection or mortality (Tables S5, S6), we found a significantly greater proportion of persistent fungemia among candidemic patients carrying the C allele (22%) compared to those carrying the GG genotype (8%) (*P*=0.011; OR, 3.27; 95% CI, 1.32–8.47)(Figure 6I; Table S7). In a multivariate model that controlled for confounding clinical factors, the presence of the C allele remained independently associated with persistent fungemia (*P*=0.02; aOR, 3.12; 95% CI, 1.20–8.42) (Figure 6J; Table S7). Total parenteral nutrition was the only other risk factor associated with persistent fungemia in both univariate and multivariate analyses (Figure 6J;

Table S7). Therefore, these data show that a *C5* SNP, which decreases *C5* mRNA levels in PBMCs, is independently associated with persistent fungemia in candidemic patients.

Lower serum C5a is an independent risk factor for death in candidemic patients

To determine whether the observed transcription of proximal complement pathway component genes in candidemic patients (Figure 1C) was also reflected in complement activation at the protein level, we assessed serum C5a concentrations in 174 candidemic patients and compared them with 103 non-candidemic hospitalized patients and 33 healthy controls (Table S4). Candidemic patients exhibited significantly greater serum C5a (mean, 29.3 ng/mL; range, 0–123.8 ng/mL) compared to both healthy donors (mean, 2.9 ng/mL; range, 0–11.8 ng/mL) and non-candidemic hospitalized patients (mean, 11 ng/mL; range, 0–33.2 ng/mL) (Figure 7A). Because serum C5a concentrations varied substantially among candidemic patients, we wondered whether the magnitude of serum C5a present at the diagnosis of candidemia is related to poorer clinical outcomes[46,47]. We used maximally selected rank statistics[80–82] and identified an optimal cut-off threshold for serum C5a of 34.7 ng/mL to classify patients as $C5a^{lo}$ (<34.7 ng/mL) or $C5a^{hi}$ (≥34.7 ng/mL). Although there was no association of $C5a^{lo}$ status with persistent fungemia or disseminated infection (Tables S5, S7), $C5a^{lo}$ candidemic patients exhibited significantly greater 90-day mortality (36%) compared to $C5a^{hi}$ candidemic patients (16%) (P=0.007; HR, 2.58; 95% CI, 1.26–5.3)(Figures 7B–C; Table S6). We built a multivariate Cox proportional hazards regression model to evaluate the association between $C5a^{lo}$ status and mortality after adjusting for confounding clinical factors including age, cancer, hemodialysis, liver disease, heart disease, cancer, neutropenia, WBC >15, solid organ transplantation, and immunocompromised status (Figure 7B; Table S6). In the multivariate model, $C5a^{lo}$ status (P=0.033; aHR 2.36; 95% CI, 1.07–5.17) and cancer (P=0.0011; aHR 2.89; 95% CI, 1.49–5.61) were the only factors independently associated with increased mortality in candidemic patients (Figures 7B–C; Table S6). Collectively, these data corroborate activation of the complement cascade to generate biologically-active fragments in candidemic patients and indicate that suboptimal induction of C5a is an independent risk factor for mortality.

Discussion

Herein, we identify a critical role for C5a-C5aR1-dependent phagocyte activation in defense against systemic fungal infection. We show that complement transcriptional induction is predictive of human candidemia and that suboptimal complement activation correlates with unfavorable outcomes in candidemic patients. Mechanistically, C5aR1 mediates neutrophil fungal uptake and macrophage survival, accumulation, and killing, which promotes fungal clearance and host survival. Our conclusions are based on extensive analyses of clinical, microbiological, pathological, immunological, transcriptional, imaging, metabolic, biochemical, and molecular parameters between WT and *C5ar1*$^{-/-}$ mice and corroborating immunological, transcriptional, and genetic investigations in patients. Our study identifies locally-produced, phagocyte-derived C5 as a key mediator of antimicrobial function that protects during systemic infection and uncovers the mechanisms underlying susceptibility of eculizumab-treated patients to fungal disease.

Early *Candida* growth restriction by renal phagocytes critically protects against systemic candidiasis[6,46,54,83]. We show that C5ar1 exerts pleiotropic, non-canonical, phagocyte functions that curtail fungal growth and filamentation, a known virulence trait[2]. First, C5aR1 mediates macrophage accumulation by providing ERK1/2- and AKT-dependent survival signals and inhibiting apoptosis and pyroptosis. Second, C5aR1 promotes renal neutrophil fungal uptake, consistent with C5aR1-regulated neutrophil fungal uptake in the murine pulmonary vasculature and in a human blood infection model[84,85]. The decreased expression of Dectin-1 and Fcγ R1 in *C5ar1*$^{-/-}$ renal and BM neutrophils extends the reported C5aR1-regulated expression of Fcγ Rs in alveolar, peritoneal, and liver macrophages during sterile inflammation and hemolysis[86–89]. Third, C5aR1 promotes macrophage fungal killing. These qualitative and quantitative defects of *C5ar1*$^{-/-}$ renal phagocytes collectively instigate early, inexorable fungal growth and filamentation.

Moreover, we show that *C5ar1*$^{-/-}$ renal macrophages exhibit enhanced mTORC1 activity and metabolic rewiring. Prior work implicated C3-C3aR on T cells and synovial fibroblasts in promoting mTORC1 activation, indicative of cell type- and context-specific mTORC1 regulation by different complement effectors[90,91]. How C5a-C5aR1 negatively regulate macrophage mTORC1 activation during candidiasis remains unknown. Hyperactive mTORC1 can induce apoptosis and pyroptosis[71,72,92]. Hence, rapamycin-induced inhibition of hyperactive mTORC1 in *C5ar1*$^{-/-}$ mice reduced macrophage death and improved survival and kidney function post-candidiasis. In agreement, mice with constitutively-activated mTORC1 exhibited increased macrophage death and susceptibility to systemic candidiasis[93]. Similarly, rapamycin-mediated mTORC1 inhibition during LPS-induced endotoxemia protected mice during secondary fungal challenge[94]. These data suggest that hyperactive mTORC1 can be deleterious during severe systemic candidiasis and its pharmacological inhibition could be beneficial. Notably, during non-lethal *Candida* challenge, mTORC1-dependent metabolic rewiring protected against subsequent candidiasis in a model of trained immunity[95]. These observations underscore the context-specific biological functions of mTORC1 during systemic fungal challenge.

Although the liver is a well-established source for complement proteins, extrahepatic, leukocyte- and stromal cell-intrinsic intracellular complement production (“the complosome”) is increasingly recognized to exert immunological, metabolic, and biological functions during inflammation[14,16,96,8,15,97]. For example, intracellular C3 in synovial fibroblasts perpetuated inflammatory arthritis and intracellular C3 in lung epithelial cells promoted or ameliorated lung immunopathology during SARS-CoV2 or *Pseudomonas* infection, respectively[12,90,98]. C3 also promotes SARS-CoV2-driven immunopathology and fatal patient outcomes via T cell activation[99]. Moreover, intracellular C5 in lymphocytes and monocytes/macrophages mediates Th1 and IL-1β responses, respectively, and the latter worsened sterile inflammation[15,16]. However, whether cell-intrinsic, extrahepatic complement production mediates antimicrobial defense was unknown. Here, we show that phagocyte-derived, locally-produced C5 in the kidney is essential for antifungal defense *in vivo*. Our findings establish a new paradigm in immunobiology, demonstrating for the first time the direct role of cell-intrinsic complement generation for anti-*Candida* defense. They set the stage for defining a) the antimicrobial role of “the complosome” against

other pathogens[100] and b) the molecular determinants of fungal-induced phagocyte-intrinsic complement production.

While phagocyte-produced C5 is a key "complosome" component for antifungal immunity, future studies are needed to delineate whether it engages its receptor exclusively on the cell surface or interior (as in $CD4^+$ T cells), or acts in a paracrine manner on neighboring cells. Moreover, the intact fungal control in *Lyz2-Cre/C3*$^{fl/fl}$ mice is somewhat surprising as we recently showed that cell-autonomous C3 drives an intracellular C5 convertase which supports macrophage-intrinsic C5a generation for inflammasome activation[15]. However, intracellular C3 and C5 storages in monocytes are largely non-overlapping and reside in separate subcellular compartments[15], suggesting that convertase formation is tightly-regulated post-cell activation. Furthermore, we recently noted that intracellular C3 activation controls macrophage efferocytosis without affecting intracellular C5a levels[101] and C5 convertase-independent, cathepsin D-dependent intracellular C5 cleavage was observed in colon cancer cells[102]. Thus, cell-autonomous C5 activation in phagocytes during candidiasis may not require upstream C3 activation.

A key aspect of our work is the extension to human disease via, a) identifying a complement transcriptional module as predictive for candidemia; b) showing that a *C5* SNP, which is associated with decreased *C5* in PBMCs and protection from autoimmune conditions[78,79,103], independently correlates with persistent fungemia; and c) demonstrating an independent association between lower serum C5a and increased mortality post-candidemia. These findings show promise for developing individualized risk stratification and prognostication strategies and underscore the importance of vigilant surveillance for fungal infections in patients receiving C5-, C5AR1-, and C3-targeted biologics. Indeed, fungal infections have emerged with the newer FDA-approved C5-targeted antibody, ravulizumab (https://fis.fda.gov/sense/), and the FDA and EMA reported and warned against the risk of fungal disease in patients receiving the C3 inhibitor, pegcetacoplan[104,105].

Overall, our study provides mechanistic and translational insights into how C5a-C5aR1 orchestrate phagocyte-dependent immunity during fungal disease, thereby illuminating the relationship between intracellular phagocyte-intrinsic C5 production and antimicrobial defense.

Limitations of the study

We provide a detailed mechanistic analysis of C5a-C5aR1-dependent antifungal defense. The precise molecular mechanisms of C5aR1-dependent macrophage killing and C-type lectin receptor (CLR) expression regulation on neutrophils remain unknown. Because FcγRs can regulate C5 production via Fc receptor common γ chain (γFc chain)-coupled signaling[87,106] and several fungal-sensing CLRs couple with γFc-chain[107], it is important to unveil whether FcγRs and/or other molecules modulate phagocyte-intrinsic complement production post-fungal challenge. Future work is also needed to precisely delineate the mechanistic role of C3a-C3aR in defense against systemic candidiasis. As with any genetic association study, the association of *C5* SNP with persistent fungemia could be due to linkage with another SNP or population stratification bias. This finding requires validation in other patient cohorts, including other racial backgrounds.

STAR METHODS

RESOURCE AVAILABILITY

Lead contact—Further information and requests for resources and reagents should be directed to and will be fulfilled by the lead contact, Dr. Michail S. Lionakis (lionakism@niaid.nih.gov).

Materials availability—The current study did not generate any new unique reagents.

Data and code availability

- Mouse RNA-Seq data of macrophages and neutrophils from infected kidneys have been deposited at the NCBI's gene expression omnibus (GEO) and are publicly available as of the date of publication. Accession number is listed in the key resources table. This paper also analyzes existing, publicly available data; the accession numbers for these datasets are listed in the key resources table.
- This paper does not report original code.
- Any additional information required to reanalyze the data reported in this paper is available from the lead contact upon request.

EXPERIMETAL MODEL AND STUDY PARTICIPANT DETAILS

Animals—Wild-type (Balb/cJ), congenic CD45.1 (JAX strain 006584), *C5ar1*$^{-/-}$ (JAX strain 006845), *C3*$^{-/-}$ (JAX strain 029661) and *Cx3cr1-Cre*^{tg} (JAX strain 025524) were obtained from the Jackson laboratory (Bar Harbor, ME). *C5ar2*$^{-/-}$ [108], *YFP-C5*$^{fl/fl}$ [15], *tdTomato-C3*$^{fl/fl}$ [109], *Albumin-Cre*^{tg}*/C5*$^{fl/fl}$, and *Lyz2-Cre*^{tg}*/C5*$^{fl/fl}$, and *Lyz2-Cre*^{tg}*/C3*$^{fl/fl}$ mice were obtained from Dr. Claudia Kemper (NHLBI/NIH). *GFP-C5ar1*$^{fl/fl}$ and *Lyz2-Cre*^{tg}*/C5ar1*$^{fl/fl}$ mice[31] were obtained from Dr. Jorg Kohl (University of Lubeck, Germany). *GFP-C5ar1*$^{fl/fl}$ mice were crossed with heterozygous *S100a8-Cre*^{tg} (gift from Dr. Rachel Caspi, NEI/NIH) or *Cx3cr1-Cre*^{tg} mice to derive *S100a8-Cre*^{tg}*/C5ar1*$^{fl/fl}$ and *Cx3cr1-Cre*^{tg}*/C5ar1*$^{fl/fl}$ animals, respectively. For each experiment, sex-matched female or male mice were used, aged between 8 to 12 weeks. Mice were maintained under specific pathogen free conditions in individual ventilated cages and were used in studies following the recommendations in the Guide for the Care and Use of Laboratory Animals of the National Institutes of Health, under the auspices of protocol LCIM14E approved by the Animal Care and Use Committee of the NIAID.

Candida albicans culture—*C. albicans* was grown on YPD (Yeast extract/Peptone/Dextrose) agar plates for 48 hours to obtain single colonies. A single colony was then used to inoculate YPD broth containing penicillin/streptomycin (Corning, NY) and was grown for 16–24 hours at 30°C. Following two serial passages, yeast cells were centrifuged, washed twice with sterile PBS, and reconstituted in PBS for downstream use.

Mouse models of candidiasis—The *Candida albicans* strains SC5314[46], CAF2–1-dTomato[46], and a isogenic rapamycin-resistant *rbp1Δ/Δ* strain[74] were used in the present study. A previously described model of systemic candidiasis was used [21,22], in which 75,000

C. albicans blastospores were injected via the mouse lateral tail vein. To assess the impact of C5a or C3a treatment on the outcome of murine systemic candidiasis, WT mice received two doses of 500 ng of C5a or C3a (R&D Systems, Minneapolis, MN) dissolved in PBS retroorbitally; the first dose was 8 hours before infection and the second dose was 24 hours post-infection. For oropharyngeal and vulvovaginal candidiasis experiments, sublingual or vaginal inoculations and fungal burden determinations were performed as described previously [110,111]. In brief, for oropharyngeal candidiasis, *C. albicans* was resuspended at 10^7/mL in PBS. The infection was carried out by placing the cotton swabs, soaked in the fungal suspension, for 90 minutes while the mice were anesthetized with ketamine and xylazine. For vulvovaginal candidiasis, three days prior to the infection, the mice were treated with 0.5 mg β-estradiol (Millipore Sigma, Burlington, MA) subcutaneously. Subsequently, 5×10^6 *Candida* in 20 μL PBS were directly inoculated to the vaginal lumen.

Generation of bone marrow radiation chimeras—Femurs and tibias were harvested aseptically from CD45.2$^+$ *C5ar1*$^{-/-}$ and congenic CD45.1$^+$ *C5ar1*$^{+/+}$ mice. The bones were flushed using PBS + 2mM EDTA. Following two washes with PBS, the cells were resuspended in PBS for injection. The 6–8 week old recipient mice were irradiated with two cycles of 4.5 Gy, spaced 4 hours apart. After 4 hours of the second irradiation, 5×10^6 bone marrow cells were injected into each recipient mouse via the lateral tail vein. To generate mixed bone marrow radiation chimeras, CD45.1$^+$ *C5ar1*$^{+/+}$ and CD45.2$^+$ *C5ar1*$^{-/-}$ bone marrow cells were mixed at a 1:1 ratio and 5×10^6 bone marrow cells were injected into recipient CD45.1$^+$ *C5ar1*$^{+/+}$ mice. The recipient mice were given trimethoprim-sulfamethoxazole in the drinking water for 4 weeks after transplantation and then subsequently switched to antibiotic-free water. Chimerism was analyzed in blood at 9 weeks after transplantation. At 10 weeks after transplantation, the mice were infected with *C. albicans* for survival and fungal burden determination, as described above, or determination of myeloid phagocytes in blood and kidney, as described below.

Rapamycin treatment of mice—Mice were treated with vehicle or rapamycin, intraperitoneally, starting at 24 hours post-infection. 150 μg of rapamycin (MedChem Express, Monmouth Junction, NJ) per mouse was administred in 200 μl of sterile vehicle (5% polyethylene glycol 400 + 5% Tween-80, both in-vivo-use grade, in USP Water for Injection); dosing was continued once daily for up to 14 days post-infection.

Human participants, specimens, and data—Patients with candidemia and non-candidemic controls were enrolled after informed consent (or waiver as approved by the Institutional Review Board (IRB)) at the Duke University Hospital (DUMC) between 2003 and 2009. To allow for similar co-morbidities and clinical factors, non-infected patients were recruited from the same hospital wards as the infected patients. The study was approved by the IRB at DUMC and was performed in accordance with the Declaration of Helsinki. Participants were excluded where sufficient clinical data or blood volume were unavailable. Additionally, patients with allogeneic hematopoietic stem cell transplant were excluded. The candidemic patients were followed prospectively to assess their clinical outcomes such as disseminated infection, persistent fungemia and mortality. Disseminated candidiasis was defined as the presence of *Candida* species at normally sterile body sites

other than the bloodstream or urine. Persistent fungemia was defined as 5 or more days of persistently positive blood cultures. Immunocompromised status was defined as the presence of any of the following: neutropenia (<500/mm^3), lymphopenia (absolute $CD4^+$ T cell counts <250/mm^3, associated with/without HIV), chronic corticosteroid use or receipt of immunosuppressive chemotherapy or other immunosuppressant medications within 30 days prior to diagnosis, diabetes mellitus, and/or end-stage renal disease requiring hemodialysis. De-identified serum specimens were obtained from 174 candidemic patients and 103 non-candidemic controls as approved under the IRB protocol Pro00047972 to quantify the serum concentrations of C5a. Additionally, serum samples from 33 healthy donors, who were enrolled in the NIAID (clinicaltrials.gov, NCT01386437) IRB–approved protocol were also included in the analysis.

To assess the association between complement transcriptional module induction and clinical outcomes of patients with candidemia, previously published public transcriptional data were sourced, as deposited under the accession number GSE176262. These patients constitute an independent cohort, as the participants were recruited at DUMC from 2011 to 2014. We obtained corresponding de-identified clinical outcome data as approved under the IRB protocol Pro00047972.

Human macrophage culture—Human elutriated monocytes were obtained from healthy donors on an IRB-approved NIH protocol (99-CC-0168). Research blood donors provided written informed consent, and blood samples were de-identified prior to distribution (NCT00001846). The monocytes were allowed to adhere to wells of a 6-well cell culture plates for 2 hours at 37 °C with 5% CO_2. Then, the non-adherent cells were washed off and macrophage differentiation medium was added to each well and the cells were incubated at 37 °C with 5% CO_2 for 5 days, at which point the old growth medium was replaced by fresh medium. The incubation was continued for an additional two days. Then, the non-adherent cells were washed off with two gentle washes with PBS and the adherent macrophages were harvested using a cell lifter and addition of EDTA-containing medium.

Murine bone marrow macrophage culture—Bone marrow cells, harvested as above, were resuspended in RPMI containing 20% FBS, penicillin/streptomycin and 40 ng/mL mouse M-CSF (Peprotech, Cranbury, NJ). Cells were plated on 75 cc tissue culture flasks and incubated for 3 days at 37°C with 5% CO_2 at which point the growth medium was replaced with fresh medium. The incubation was continued for an additional two days. Subsequently, the growth medium was removed, non-adherent cells were washed with two gentle washes with PBS, and the adhered macrophages were harvested using a cell lifter.

METHOD DETAILS

Fungal burden determination in murine tissues—To determine tissue fungal burden, the kidney, spleen, liver, heart, lungs, brain or tongue were harvested at specified time-points, aseptically weighed and homogenized using Omni Tip homogenizers (Omni International, Kennesaw, GA). Vaginal lavage fluid was quantified in mice with vulvovaginal candidiasis. The tissue homogenates or vaginal lavage fluid were then plated on YPD agar plates and incubated at 37°C for 48 hours for CFU enumeration.

Serum blood urea nitrogen & creatinine assay—Blood was harvested from anesthetized mice via cardiac puncture. Serum was separated using serum gel tubes (SAI Infusion Technologies, Lake Villa, IL) and stored at −80°C until use. Serum blood urea nitrogen and creatinine were analyzed using commercially available Quantichrom urea and creatinine assay kits from BioAssay Systems (Hayward, CA).

Histological analysis of kidneys—At specified timepoints after infection, the right kidneys from mice were harvested and placed in 10% buffered formalin overnight for fixation. Subsequently, formalin was decanted and was replaced with 70% ethanol. Paraffin-embedding, sectioning and staining with Periodic acid-Schiff stain were performed at Histoserve Inc (Gaithersburg, MD).

Neutrophil isolation and ROS assay—Femurs and tibias were harvested aseptically, and the bones were flushed using RPMI with 10% FBS and penicillin/streptomycin. Following red blood cell lysis using ACK lysing buffer, the bone marrow cells were washed with PBS and resuspended in MACS buffer (PBS containing 5% bovine serum albumin). To isolate neutrophils, kidneys at day 2 post-infection were harvested, and a single cell suspension was prepared as described below. Neutrophils were isolated from the bone marrow or the kidney single suspensions using the Anti-Ly6G MicroBeads Ultrapure (Miltenyi Biotec, Gaithersburg, MD), as per the manufacturer's protocol. The MACS-sorted neutrophils were >95% pure as assessed by flow cytometry. To assess ROS production, a dihydrorhodamine-based assay was used[47], where the renal neutrophils were stimulated with 1 mg/mL serum-opsonized zymosan or left untreated, and the rhodamine fluorescence was assessed by flow cytometry.

Neutrophil fungal uptake assay—5×10^6 blastospores of dTomato$^+$ *C. albicans* [112] were opsonized with 10% v/v mouse serum and were added to capped round-bottomed polystyrene tubes (Corning, Glendale, AZ) containing 5×10^6 MACS-sorted bone-marrow neutrophils. In experiments assessing the effects of C5a or C3a on neutrophil fungal uptake, neutrophils were treated with 100 ng/mL C5a or C3a (R&D Systems, Minneapolis, MN) for 15 minutes at 37°C, before infecting with *Candida*. After 30 minutes incubation in a shaking waterbath set at 37°C, the tubes were transferred on ice and stained using an antibody against mouse CD11b (clone M1/70, Biolegend, San Diego, CA). The cells were then analyzed using a 5-laser LSRFortessa flow cytometer (BD Biosciences, Franklin Lakes, NJ). The neutrophil associated *Candida* was visualized as CD11b$^+$/dTomato$^+$. The data were exported to FlowJo (BD Biosciences, Franklin Lakes, NJ) for further analysis.

Macrophage fungal killing assay—*Candida* killing was assessed, as described previously [46], in the presence of normal serum (5% v/v). Briefly, 10^5 macrophages were seeded in 96-well plates and incubated overnight at 37 °C in a humidified incubator containing 5% CO_2. The next day opsonized *Candida* yeast cells (5×10^5 yeast cells; opsonized with 10% v/v mouse serum) were added to the macrophages. In experiments assessing effects of C5a or C3a on macrophages' *Candida* killing capacity, macrophages were treated with 100 ng/mL C5a or C3a (R&D Systems, Minneapolis, MN) for 1 hour before infecting with *Candida*. After 3 hours of incubation with *Candida*, the macrophages

were lysed with 0.02% Triton-X-100, washed twice with PBS and incubated with Alamar Blue reagent (Thermo Fisher, Waltham, MA) for 18 hours at 37 °C in a humdified incubator containing 5% CO_2. Alamar Blue fluorescence, indicative of viable *Candida* was recorded and the macrophage killing capacity was calculated by comparing the fluorescence of wells containing *Candida* with macrophages to the corresponding wells containing *Candida* without macrophages.

Avacopan in ex vivo assays—Avacopan (MedChem Express, Monmouth Junction, NJ) was used at a concentration of 500 nM. Human peripheral blood neutrophils and monocyte-derived macrophages were pre-treated with avacopan for 30 minutes and then incubated with serum-opsonized *C. albicans*. Normal serum was maintained at a final concentration of 5% v/v. Treated cells were then used for fungal uptake or killing assays as described below.

Human neutrophil isolation—Human neutrophils were obtained from heparinized blood of healthy donors at the NIH Blood Bank or from healthy donors who were enrolled in protocols approved by the NIAID IRB committees, and provided written informed consent for participation in the study. PBMCs were first separated using Lymphocyte Separation Medium (Lonza, Rockville, MD), as per the manufacturer's instructions. Neutrophils were then sedimented using 3% dextran in 0.85% NaCl, followed by red blood cell lysis using NaCl, and isolated neutrophils were then used to assess *C. albicans* phagocytosis as described above [47]. Briefly, 5×10^6 blastospores of dTomato$^+$ *C. albicans* [114] were opsonized with 10% v/v human serum and were added to capped round-bottomed polystyrene tubes (Corning, Glendale, AZ) containing 5×10^6 neutrophils. After 30 minutes incubation in a shaking waterbath set at 37°C, the tubes were transferred on ice and stained using an antibody against human CD15 (clone HI98, Biolegend, San Diego, CA). The cells were then analyzed using a 5-laser LSRFortessa flow cytometer (BD Biosciences, Franklin Lakes, NJ). The neutrophil associated *Candida* was visualized as CD15$^+$/dTomato$^+$. The data were exported to FlowJo (BD Biosciences, Franklin Lakes, NJ) for further analysis.

Kidney single cell suspension preparation—Single cell suspension from mouse kidneys were prepared as described previously [46]. In brief, the kidneys were aseptically isolated, digested in digestion medium (RPMI with 25mM HEPES) containing DNase (10104159001; Milipore Sigma, Burlington, MA) and liberase TL (05401020001; Milipore Sigma, Burlington, MA) and minced into <1mm pieces. The kidney pieces were then transferred into a 50 mL conical tube containing 10 mL digestion medium and incubated at 37 °C for 20 minutes with shaking. The digestion was then halted by adding ice-cold RPMI containing 10% FBS and 25 mM HEPES and the digested tissue suspension was passed through 70 μm cell strainer, washed, and treated with ACK lysing buffer for red blood cell lysis. The suspension was then passed through a 40 μm cell strainer, washed once, and resuspended in 40% Percoll (GE17–0891-01; Milipore Sigma, Burlington, MA), overlaid onto 70% Percoll, and centrifuged at 939 ×g for 30 minutes at room temperature. The kidney single cell suspension was harvested from the interface of 40% and 70% Percoll, washed twice, and used in downstream applications.

Murine kidney immunophenotyping—Kidney single cell suspensions was prepared above, and a small fraction was fixed with 2% paraformaldehyde for determination of absolute leukocyte numbers using PE-conjugated counting beads, as previously described (Spherotech, Lake Forest, IL) [22]. The remainder of the single cell suspension was first stained with LIVE/DEAD Fixable Blue Dead Cell Stain (Thermo Fisher, Waltham, MA) at 1:200 dilution) for 10 minutes on ice. Then, rat anti-mouse CD16/CD32 (clone 2.4G2; BD Biosciences, Franklin Lakes, NJ), was added at 1:100 dilution together with 0.5% bovine serum albumin and the cells were incubated on ice for 10 minutes. The following fluorochrome-coupled antibodies against specific cell surface antigens were then added at 1:100 dilution: CD45 (clone 30-F11, Biolegend, San Diego, CA), Ly6G (clone 1A8, Biolegend), CD11b (clone M1/70, Biolegend, San Diego, CA), CD11c (clone N418, Thermo Fisher, Waltham, MA), Ly6C (clone AL-21, BD Biosciences, Franklin Lakes, NJ), CD103 (clone 2E7, Biolegend, San Diego, CA), MHCII (clone M5/114.15.2, Thermo Fisher, Waltham, MA), F4/80 (clone BM8, Biolegend, San Diego, CA), CD3 (clone 145–2C11, Biolegend, San Diego, CA), CD19 (clone 1D3, Biolegend, San Diego, CA), CD31 (clone MEC13.3, Biolegend, San Diego, CA), and NKp46 (clone 29A1.4, Biolegend, San Diego, CA). The cells were incubated with antibodies on ice for 30 minutes, washed thrice with FACS buffer (PBS containing 5% bovine serum albumin and 0.1% NaN_3), and passed through 35 μm cell strainer. The cells were then analyzed using a 5-laser BD LSR Fortessa II (BD Biosciences, Franklin Lakes, NJ) and data were collected using FACS Diva (BD Biosciences, Franklin Lakes, NJ) and analyzed using FlowJo (BD Biosciences, Franklin Lakes, NJ).

Determination of renal macrophage apoptosis—Kidney single cell suspensions were prepared from the infected kidneys of *C5ar1*$^{+/+}$ and *C5ar1*$^{-/-}$ mice at day 1 post-infection and stained as above. In experiments assessing the role of rapamycin treatment on apoptosis, *C5ar1*$^{-/-}$ kidneys were harvested at day 3 after infection with SC5314 or the isogenic rapamycin-resistant *rbp1Δ/Δ Candida* strains. After washing off the excessive unbound fluorochrome-coupled antibodies, the cells were resuspended in Annexin Binding buffer (Thermo Fisher, Waltham, MA), to which FITC-conjugated Annexin V (Thermo Fisher, Waltham, MA) and Propidium iodide (BD Biosciences, Franklin Lakes, NJ) were added. After 15 minutes of incubation at room temperature, additional Annexin Binding buffer was added to the cells and the cells were quickly analyzed via flow cytometry, as described above.

Determination of bone marrow-derived macrophage apoptosis—In *in vitro* experiments assessing bone marrow-derived macrophage apoptosis, 10^5 macrophages were seeded in 96-well plates in RPMI + 1% FBS and incubated overnight at 37 °C in a humidified incubator containing 5% CO_2. The next day the cells were treated with C5a or C3a (100 ng/mL; R&D Systems, Minneapolis, MN) with or without AS-252424 (0.1 μM), U0126 (10 μM) or rapamycin (0.1 μM). After 1h, the macrophages were infected with 10^5 *rbp1Δ/Δ Candida;* in experiments involving C5a or C3a, an additional 100/ ng/mL C5a or C3a was added at 2.5h after infecting with *Candida*. After 5h incubation, apoptosis and cell survival of the macrophages were assessed as described in the section above.

Renal phagocyte isolation for RNA-Seq—Single cell suspensions were prepared from *C5ar1*$^{+/+}$and *C5ar1*$^{-/-}$ kidneys of mice infected with *C. albicans* at day 2 post-infection. Macrophages and neutrophils were stained using sterile anti-mouse antibodies against CD45 (clone 30-F11, Biolegend), Ly6G (clone 1A8, Biolegend), CD11b (clone M1/70, Biolegend), MHCII (clone M5/114.15.2, Thermo Fisher), F4/80 (clone BM8, Biolegend), CD3 (clone 145–2C11, Biolegend), CD19 (clone 1D3, Biolegend), and NKp46 (clone 29A1.4, Biolegend). Macrophages were defined as CD45^{+} CD3/CD19/NKp46/Ly6G^{-} MHCII^{hi} F4/80^{+} CD11b^{+} , while and neutrophils were defined as CD45^{+} Ly6G^{+} CD11b^{+} and were FACS-sorted with purity of >90% into RPMI supplemented with 10% FBS and penicillin/streptomycin. The sorted cells were centrifuged at 300 ×g for 5 minutes at 4 °C, resuspended in TRIzol (Thermo Fisher Scientific, Waltham, MA) and and stored at −80 °C until further use.

RNA-seq of renal phagocytes—RNA was isolated from FACS-sorted cells using TRIzol reagent (Thermo Fisher, Waltham, MA), and further processed using a RNA Clean-Up and Concentration Micro-Elute kit (cat# 61000, Norgen Biotec, ON, Canada), according to the manufacturer's guidelines. cDNA was amplified using the SMART-Seq v4 UltraLow Input RNA kit (Takara Bio, San Jose, CA) and sequencing libraries were prepared using the Nextera XT (Illumina, San Diego, CA). Multiplexed libraries were sequenced in a HiSeq3000 instrument (Illumina, San Diego, CA) in 50-bp single-end mode and mapped using STAR (v2.5.2) [113]. Gene-level counts were filtered to remove low-expression genes (keeping genes with >15 counts in at least one sample). Differential gene expression was evaluated using limma [114]. Differentially expressed genes were defined as genes with a fold change of at least 2 in either direction at false discovery rate (FDR) less than 0.01. Differentially expressed genes for macrophages and neutrophils are shown in Tables S3A–B. Pathway enrichment analysis for differentially expressed genes of *C5ar1*$^{-/-}$ versus *C5ar1*$^{+/+}$ phagocytes was performed using GSEA [18]. The genesets were sourced from *Hallmark* pathway genes curated by MSigDB [19] for macrophages, and significantly enriched pathways in *C5ar1*$^{-/-}$ macrophages are shown in Table S3C. For neutrophils, "positive regulation of phagocytosis" genes, curated by gene ontology (GO: 0050766), were used to assess for enrichment of this pathway by GSEA. The mouse RNA-seq datasets are available from the NCBI's gene expression omnibus (GEO), under accession number GSE206205.

Assay of H_2O_2 production by renal macrophages—Macrophages from the infected kidneys were flow-sorted on day 2 post-infection, as described above. Amplex™ Red Hydrogen Peroxide/Peroxidase Assay Kit (Thermo Fisher Scientific, Waltham, MA) was used to assess H_2O_2 production. Briefly, 2×10^4 cells were seeded in 96-well plates along with 0.1 U/mL horseradish peroxidase. The cells were either left untreated or treated with serum-opsonized zymosan (1.2 mg/mL) and the appearance of the fluorescent resofurin was monitored every 2.5 minutes for the duration of 2h. The fluorophore was excited at 530 nm and emission was recorded at 590 nm. Using H_2O_2 serial dilutions, a standard curve of resofurin fluorescence vs. H_2O_2 concentrations was constructed and was used to interpolate the H_2O_2 generated by the seeded renal macrophages.

Quantification of citrullinated H3 in kidneys—Immunofluorescence confocal microscopy was performed using 5 μm sections of decalcified and paraffin embedded kidneys. Antigen retrieval in 10 mM citric acid buffer was used, and sections were blocked with 2% bovine serum albumin in phosphate buffered saline (PBS) for 1 h. Sections were incubated with primary antibodies at 1:500 dilution [anti-Ly6G: BD Pharmingen™ 551459; anti-Cit-H3: ab5103] O/N at 4 °C and washed in PBS (3 times). Secondary antibody (Rhodamine Red-X anti-rat, JacksonImmuno 712–296-150; Alexa Fluor® 647-conjugated AffiniPure F(ab')2 anti-rabbit, JacksonImmuno 711–606-152; 1:500) and DAPI (1:500) were added for 1 h at room temperature. Sections were then washed in PBS (3 times), and #1.5 cover slips were mounted with ProLong™ Gold Antifade Reagent (Thermo Fisher Scientific). Images were captured on an inverted Nikon A1R+ confocal microscope (10x-air) using NIS-Elements software (Nikon), stitched and maximum intensity projected.

To quantify the Cit-H3-stained area in the kidney, a statistical threshold (set at 2 standard deviations above the mean of the image histogram) was set. The whole kidney was considered as the region of interest, and the percent citH3-stained area was reported. The analysis was performed with FIJI [115], and results were displayed as mean ± SEM.

Intracellular staining and flow cytometry—At day 2 post-infection, kidney single cell suspensions were prepared as above, and the cells were fixed by incubating for 15 minutes at room-temperature with 2% paraformaldehyde (Fisher Scientific, Pittsburgh, PA). The fixed cells were then centrifuged at 350 ×g for 6 min, paraformaldehyde was removed, and the cells were washed with ice-cold PBS. The fixed cells were then permeabilized using 100% ice-cold methanol (Fisher Scientific, Pittsurgh, PA). After 30 minutes of incubation in methanol at −80°C, the cells were washed once with ice-cold PBS. After two additional washes with FACS buffer (PBS containing 0.5% bovine serum albumin and 0.01% NaN_3), cells were incubated with rat anti-mouse CD16/CD32 (clone 2.4G2; BD Biosciences), at 1:100 dilution along with 0.5% BSA for 5 minutes at room temperature. Then, cells were incubated with anti-mouse antibodies against various cell surface markers as well as intracellular proteins such as Bax (cat 14796, clone D3R2M; Cell Signaling, Danvers, MA), cleaved caspase-3 (cat 9661, polyclonal, Cell signaling), p-Mlkl (cat 196436, clone EPR9515(2), Abcam, Cambridge, UK), Gpx4 (cat 125066, clone EPNCIR144, Abcam), p-S6 (cat 5364, clone D68F8, Cell Signaling, Danvers, MA), Glut1 (cat 115730, clone EPR3915, Abcam, Cambridge, UK), Rabbit IgG isotype (cat 02–6102, Thermo Fisher, Waltham, MA), CD45 (clone 30-F11, Biolegend, San Diego, CA), Ly6G (clone 1A8, Biolegend, San Diego, CA), CD11b (clone M1/70, Biolegend, San Diego, CA), MHCII (clone M5/114.15.2, Thermo Fisher, Waltham, MA), F4/80 (clone BM8, Biolegend, San Diego, CA), CD3 (clone 145–2C11, Biolegend, San Diego, CA), CD19 (clone 1D3, Biolegend, San Diego, CA), and NKp46 (clone 29A1.4, Biolegend, San Diego, CA). Appropriate rabbit IgG isotype controls at the same concentration of the primary intracellular antigen binding antibody were also used in parallel. The cells were then washed twice with FACS buffer (PBS containing 0.5% BSA and 0.01% NaN_3) and stained using a secondary anti-rabbit AF448-coupled antibody (cat 150077; Abcam, Cambridge, UK) along with anti-mouse CD16/CD32 and BSA, as above. After 30 minutes of incubation at room

temperature, the cells were washed twice with FACS buffer, resuspended in FACS buffer and analyzed flow cytometrically as described above.

Assay of Dectin-1/FcγR1 on renal neutrophils—Kidney single cell suspensions were prepared from *C5ar1*$^{+/+}$ and *C5ar1*$^{-/-}$ mice at day 2 post-infection and cell staining was carried out as described above. Specifically, to assess Dectin-1 and FcγR1, the cells were incubated with the following antibodies for 30 minutes on ice: Dectin-1 (clone 2A11, Bio-Rad, Hercules, CA), FcγR1 (clone X54–5/7.1, Biolegend, San Diego, CA), CD45 (clone 30-F11, Biolegend, San Diego, CA), Ly6G (clone 1A8, Biolegend, San Diego, CA), CD11b (clone M1/70, Biolegend, San Diego, CA), MHCII (clone M5/114.15.2, Thermo Fisher, Waltham, MA), F4/80 (clone BM8, Biolegend, San Diego, CA), CD3 (clone 145–2C11, Biolegend, San Diego, CA), CD19 (clone 1D3, Biolegend, San Diego, CA), and NKp46 (clone 29A1.4, Biolegend, San Diego, CA). Following two washes with FACS buffer, resuspended cells were analyzed flow cytometrically as described above.

Assay of Dectin-1/FcγR1 on bone marrow neutrophils—5×10^6 MACS-sorted bone-marrow neutrophils were transferred to capped round-bottomed polystyrene tubes (Corning, Glendale, AZ) and were left untreated or treated-with 100 ng/mL C5a (R&D Systems, Minneapolis, MN) for 15 minutes at 37°C. To assess whether *Candida* can impact Dectin-1/FcγR1 expression and whether C5a can further affect *Candida*-dependent Dectin-1/FcγR1 expression, 5×10^6 opsonized *Candida* yeast cells were added to the tubes containing neutrophils, with or without C5a. After 30 minutes of incubation in a shaking waterbath set at 37°C, the tubes were transferred on ice and stained using antibodies against mouse CD11b (clone M1/70, Biolegend, San Diego, CA), Dectin-1 (clone 2A11, Bio-Rad, Hercules, CA), and FcγR1 (clone X54–5/7.1, Biolegend, San Diego, CA). Following two washes with FACS buffer, resuspended cells were analyzed using a 5-laser LSRFortessa flow cytometer (BD Biosciences, Franklin Lakes, NJ). The neutrophils were identified as a CD11b$^+$ population and the geometric mean fluorescence intensity of Dectin-1 and FcγR1 was assessed.

Assay of fungal association and killing in vivo—5×10^8 blastospores of dTomato$^+$ *C. albicans* [112] were incubated with 0.5 mg/mL Biotin-XX-SSE (Fisher Scientific, Pittsburgh, PA) in 50 mM sodium carbonate buffer for 2 h in a microtube shaker. Excess Biotin-XX-SSE is then removed by washing twice with 0.1 M Tris-HCl, following which the *Candida* was incubated with 0.02 mg/mL streptavidin conjugated to Alexa Fluor 633 (Cat S21375; Thermo Fisher, Waltham, MA) in PBS, in dark for 30 minutes. After washing off excess flurophore, the labled *Candida* was used to infect mice, where 5×10^6 CFU of the labeled *Candida* was injected via lateral tail vein. At 2 hours post-infection, the kidneys were harvested for single cell suspension preparation and staining as described above. The stained kidney cells were analyzed using a 5-laser LSRFortessa flow cytometer (BD Biosciences, Franklin Lakes, NJ). After gating on live phagocyte subset, the phagocyte associated *Candida* was visualized as AF633$^+$/dTomato$^+$ (live) or AF633$^+$/dTomato$^-$ (dead). The data were exported to FlowJo (BD Biosciences, Franklin Lakes, NJ) for further analysis.

Intravital microscopy of kidney—The left kidney of an anesthetized *C5ar1*$^{+/+}$ or *C5ar1*$^{-/-}$ mouse (isoflurane/oxygen delivered using a custom-made nosecone) was exteriorized through a ~0.5 cm retroperitoneal incision on the left flank. The exteriorized kidney was placed on a cover-glass of the pre-warmed microscope stage-insert; immediately pre-warmed PBS-soaked Kimwipe (Kimberley-Clark, Irving, TX) was placed over the exposed tissue to prevent dehydration (300 μL saline was applied every 15 minutes during imaging session). Subsequently, 5×10^6 dTomato expressing *C. albicans* [112], 5 μg of anti-mouse BV421-conjugated CD31 (clone 390, Biolegend, San Diego, CA), 2.5 μg of anti-mouse AF488-conjugated F4/80 (clone BM8, Biolegend, San Diego, CA) and 2 μg of anti-mouse APC-conjugated Ly6G (clone 1A8, Biolegend, San Diego, CA) were injected retro-orbitally. Immediately upon injection, the mouse was transferred onto the microscope. Microscopy was performed immediately using a Leica SP8 Dual MP microscope. The fluorophores were excited using 405nm/488nm/594nm/633nm laser lines. Image stacks of upto 90 μm thickness were acquired every 2 to 2.5 minutes, with Δz of 2 μm using a 25X 0.95 NA water immersion objective (xyz voxel size of 0.303 μm, 0.303 μm, and 1.999 μm, respectively). The images were exported to FIJI [115], where the stacks were processed to remove 3D drift. The processed image stacks were then exported to Bitplane Imaris 9.0, where the surface creation module was used to segment BV421$^+$ vasculature, AF488$^+$ macrophages, dTomato$^+$ *Candida* and Ly6G$^+$ neutrophils. For Ly6G$^+$ neutrophil surfaces, the analyses of sphericity, number of segmented neutrophils per timeframe and velocity were exported to Microsoft Excel.

To assess germination frequency, the processed images were analyzed at 1 hour post-infection and the germinated *Candida* were enumerated to determine germination frequency. To assess fungal association with neutrophils or macrophages, a uniform temporal window of 30 minutes within the first 75 minutes post-infection was chosen and the dTomato$^+$ *Candida* showing stable association with either of the phagocytes for >3 temporal time-frames were enumerated. For such stably associated fungi, the phagocytes-fungal association lasted for an entire imaging session. The stably associated dTomato$^+$ *Candida* surfaces were then used to assess fungal growth. The number of individual *Candida* cells were marked as showing growth if they exhibited germination and/or filamentous extension of hyphae. For calculating hyphal extension rate, the hyphal length was determined at the start and at the end of imaging timeframes, and the extension rate was calculated as μm/h ($length_{end}$ - $length_{start}$/Δtime(h)). For display purposes, the image stacks were exported to FIJI, and "Maximum Intensity Projections" were computed for display. The movie file shown in Movie S1 was assembled in Adobe Photoshop.

Extracellular flux analysis—Renal macrophages were FACS-sorted from of *C5ar1*$^{+/+}$ and *C5ar1*$^{-/-}$ kidneys at day 1 post-infection, as described above. The sorted cells were resuspended in the Seahorse XF assay medium (Agilent, Santa Clara, CA) and 75,000 cells were dispensed in each well of the Seahorse XFe96 assay plate (Agilent, Santa Clara, CA), where the wells were pre-coated with 0.01% poly-L-lysine. The plate was briefly centrifuged at 45 × *g* for 5 minutes without acceleration and brake and subsequently incubated at 37°C non-CO_2 incubator for 45 minutes. During that time, the Seahorse XFe96 analyzer (Agilent, Santa Clara, CA) was calibrated and subsequently the

extracellular flux analysis was carried out to assess basal extracellular acidification and oxygen consumption rates (ECAR/OCR). Additionally, injection ports (ports A) were also loaded with opsonized heat-killed *Candida albicans* (MOI 50) and the instrument was programed to inject the stimulus at indicated time to assess stimulus-depedent changes in ECAR/OCR. The temporal ECAR/OCR data were exported to Graphpad PRISM and area under the curve (AUC) were calculated for quantitative comparison between *C5ar1*$^{+/+}$ and *C5ar1*$^{-/-}$ macrophages.

Cytokine and chemokine level determination—Kidneys were harvested from uninfected and day 1 infected *C5ar1*$^{+/+}$ and *C5ar1*$^{-/-}$ mice and homogenized in PBS containing 0.5% Tween 20 and protease inhibitor cocktail (Roche). The homogenates were clarified by centrifugation and subsequently passing through a 0.22 μm filter. The clarified homogenates were stored at −80 °C until further use. The cytokines and chemokines were analyzed using a multiplexed bead-based assay system (Luminex Corporation, Austin, TX), and the concentrations were reported per gram of the tissue [116].

Determination of C5a and C3a in sera—Serum C5a levels in humans and mice were analyzed using the Human Complement Component C5a DuoSet ELISA kit (cat DY2037, R&D Systems, Minneapolis, MN) or Mouse Complement Component C5a DuoSet ELISA kit (cat DY2150, R&D Systems, Minneapolis, MN), respectively. Serum C3a levels in mice were determined using the capture/detection antibodies and C3a standards from BD (BD Biosciences; 558250, 558251, and 558618).

qPCR-based determination of transcripts—To determine transcript levels of *C5*, *C5ar1*, *C5ar2*, the tissue were harvested at specified time-points after infection, placed in ice-cold TRIzol and homogenized using Omni tip homogenizers (Omni international, Kennesaw, GA). RNA was isolated using the RNeasy mini kit (QIAGEN, Germantown, MD), as per the manufacturer's instructions. cDNA was synthesized using qScript cDNA synthesis kit (Quanta bio, Bevereley, MA) and qPCR was performed using PerfeCTa SYBR Green Fast Mix (Quanta bio, Beverly, MA), 10ng cDNA and 100nM transcript primers, on a QuantStudio 3 Real-Time PCR System (Thermo Fisher, Waltham, MA). Transcript levels were determined relative to expression GAPDH using ΔC_T method.

Immunoblots to analyze pyroptotis markers—Macrophages from infected kidneys (at day 2 post-infection) were FACS-sorted as described above. After centrifugation at 350 ×g for 5 minutes, the cell pellet was resuspended in 1× RIPA buffer (Thermo Fisher Scientific, Waltham, MA) containing protease and phosphatase inhibitors (Thermo Fisher Scientific, Waltham, MA) for preparing lysates. For assessing pyroptosis using bone marrow-derived macrophages, 10^6 macrophages were seeded in 24-well plates and incubated overnight at 37 °C in a humidified incubator with 5% CO_2. The next day, the macrophages were infected with *Candida* SC5314 (MOI 1), with or without priming with LPS (Thermo Fisher Scientific; 50 ng/mL) for 2 hours. After 5h, the supernatant was removed, and lysates were prepared by adding 1× RIPA buffer containing protease and phosphatase inhibitors directly to the wells. Protein concentrations were quantified using the Bradford Protein Assay (Bio-Rad, Hercules, CA) and 20 μg of proteins were

resolved on 10% SDS-PAGE. The proteins were transferred onto 0.2-μm PVDF membrane, which were blocked in 5% nonfat dry milk and incubated with primary antibodies against cleaved Gsdmd (clone EPR19828, Abcam, Cambridge, UK), caspase-1 (clone D7F10, Cell Signaling), and β-actin (clone D6A8, Cell Signaling, Danvers, MA), followed by secondary anti-rabbit IgG, HRP-linked antibodies (Cell Signaling). Chemiluminescence detection was performed with Clarity Western ECL Blotting Substrate (Bio-Rad, Hercules, CA) or Radiance ECL Substrate (Azure Biosystems, Dublin, CA), using the ChemiDoc MP Imaging System (Bio-Rad, Hercules, CA). Quantitative densitometry was performed via image analysis using Image Lab 5.2 Software (Bio-Rad, Hercules, CA).

Immunoblots to analyze signaling kinases—10^6 bone marrow-derived macrophages were seeded in 24-well plates and incubated overnight at 37 °C in a humidified incubator with 5% CO_2. The next day, the macrophages were left unstimulated or stimulated with heat-killed *Candida* (MOI 5), with or without pretreatment with 100 ng/mL C5a (R&D Systems, Minneapolis, MN) for 1 hour. After stimulation with heat-killed *Candida* for 5, 10 or 20 minutes, the supernatant was removed, and lysates were prepared by adding 1× RIPA buffer containing protease and phosphatase inhibitors directly to the wells. The proteins were resolved on 10% SDS-PAGE, transferred onto 0.2-μm PVDF membranes, which were blocked in 5% nonfat dry milk and incubated with primary antibodies against p-AKT (clone D9E), total AKT (polyclonal), p-ERK1/2 (clone D13.14.4E), total ERK1/2 (polyclonal), and β-actin (clone D6A8); all from Cell Signaling (Danvers, MA). Subsequently, the membranes were probed with secondary anti-rabbit IgG, HRP-linked antibodies (Cell Signaling). Chemiluminescence detection was performed using SuperSignal™ West Atto Ultimate Sensitivity Substrate (Thermo Fisher, Waltham, MA), and the ChemiDoc MP Imaging System (Bio-Rad, Hercules, CA). Quantitative densitometry was performed via image analysis using Image Lab 5.2 Software (Bio-Rad, Hercules, CA).

Association of serum C5a and mortality post-infection—To test the hypothesis that a low serum C5a concentration has detrimental effects on patient survival, we used Cox proportional hazards (CPH) regression to model time to death. Mortality was defined as death within 90 days of the onset of candidemia. Patients were classified as having low versus high serum C5a levels using maximally selected ranked statistics to identify the optimal cutpoint of serum C5a concentration that best distinguishes survival outcomes [80–82]. We set a priori the minimal proportion of patients in each group at 25% and determined the optimal cutpoint to be 34.7 ng/mL. Using this value, we classified patients as having low (<34.7 ng/mL) versus high (>34.7 ng/mL) serum C5a concentrations and built a multivariate CPH regression model to estimate the association between low serum C5a concentrations and host survival after adjustment for potential confounding factors including patient age, cancer, hemodialysis, chronic liver disease, heart disease, neutropenia, solid organ transplantation, WBC > 15, and an immunocompromised status. Statistical significance was defined as $P < 0.05$.

rs2269067 genotyping—Candidemia patients of mixed European descent were genotyped using the Immunochip as described before [117]. These candidemic patients were enrolled after informed consent (or waiver as approved by the IRB) at the DUMC

between 2003 and 2009, and included 90 patients for whom sera were analyzed for C5a concentrations, and an additional 79 patients for whom only DNA was available for genotyping (Table S3). Genotyping data from these patients were used to assess the correlation of rs2269067 with clinical outcomes of candidemia. To examine the impact of the *C5* SNP on *C5* mRNA levels, we screened healthy donors enrolled in the NIAID IRB–approved protocol (clinicaltrials.gov, NCT01386437) and healthy donors at the NIH Blood Bank to identify individuals carrying the rs2269067. In this case, genotyping for rs2269067 was performed using a TaqMan SNP genotyping assay (assay ID C___2783678_1_, Thermo Fisher, Waltham, MA) in a 20 μL quantitative PCR reaction. Briefly, DNA was isolated from whole blood using the Gentra Puregene Blood DNA isolation kit (QIAGEN, Germantown, MD). Quantitative PCR was performed using 20 ng of DNA and PerfeCTa FastMix Low Rox (Quanta Bio, Beverley, MA) on a Quant Studio 3 Real-Time PCR system (Thermo Fisher, Waltham, MA). Results were interpreted as follows: single “VIC” signal (CC homozygous), single “FAM” signal (GG homozygous), and a mixed VIC/FAM signal (CG heterozygous).

rs2269067 & association with clinical outcomes—To investigate the association between the *C5* rs2269067 SNP and clinical outcomes such as disseminated infection, persistent fungemia, and mortality at 90 days, a dominant model of penetrance was used whereby homozygosity at the G allele (GG) was considered wild type and the presence of 1 or more C alleles (CC or CG) indicated an affected individual. The association between rs2269067 genotype and clinical outcomes was assessed using Chi-squared test. To estimate the effect size for this association, we calculated odds ratios and 95% confidence intervals using a multivariate logistic regression model that adjusted for patient age, hemodialysis, cancer, chronic liver disease, total parenteral nutrition, neutropenia, WBC > 15, solid organ transplantation, and an immunocompromised status. Statistical significance was defined as $P < 0.05$.

rs2269067 & impact on C5 transcription—Basal *C5* transcripts were anlyzed in PBMC isolated from heparinized whole blood from healthy donors enrolled in an NIAID IRB–approved protocol (clinicaltrials.gov, NCT01386437) and healthy donors at the NIH Blood Bank. Specifically, PBMC were harvested using SepMate PBMC isolation tubes (STEMCELL Technologies, BC, Canada), as per manufacturer’s directions. Isolated PBMC were directly used for RNA purification, where TRIzol (Thermo Fisher, Waltham, MA) was added to the PBMC and RNA was purified as described above using the RNA Clean-Up and Concentration Micro-Elute Kit (Norgen Biotek, ON, Canada). cDNA was synthesized using qScript cDNA synthesis kit (Quanta bio, Beverley, MA) and qPCR was performed using PerfeCTa Fast Mix Low Rox (Quanta bio, Beverley, MA), 10 ng cDNA and *C5* specific primers/probe (Hs01004342_m1, Thermo Fisher, Waltham, MA) on a QuantStudio 3 Real-Time PCR System (Thermo Fisher, Wlatham, MA). Transcript levels were determined relative to the expression GAPDH (Hs02786624_g1, Thermo Fisher, Waltham MA) using ΔC_T method.

C5 intracellular staining in human PBMC—PBMC were harvested as above, and 5×10^5 cells were incubated in round-bottom 96-well plates in RPMI + 10% FBS +

penicillin/streptomycin. PBMC were stimulated with heat-killed *Candida* (SC5314) or paraformaldehyde-fixed *Aspergillus fumigatus* (B-5233), at MOI of 10 for 16 hours, in a humidified incubator containing 5 % CO2, at 37 °C. After stimulations, the cells were fixed with 1.6% pre-warmed paraformaldehyde and permeabilized using methanol, as described previously [118]. After permeabilization, the PBMC were washed once with ice-cold PBS. After two additional washes with PBS containing 0.5% BSA (Thermo Fisher, Waltham, MA) and 0.01% NaN_3, PBMC were stained overnight at 4 °C for C5 using a rabbit antihuman C5 antibody (Abcam, Cambridge, UK), along with mouse IgG (Thermo Fisher). The next morning the PBMC were washed twice with FACS buffer (PBS + 0.5% BSA + 0.01% NaN_3) and stained using a PE-conjugated anti-rabbit antibody (BD Biosciences, Franklin Lakes, NJ) along with an antibody against human CD14 (clone MϕP9, BD Biosciences, Franklin Lakes, NJ). After 30 minutes incubation on ice, the cells were washed twice, resuspended in FACS buffer, and analyzed flow cytometrically as described above.

eQTL analysis—Genome-wide *cis*- and *trans*-eQTL data were downloaded from the eQTLGen Consortium [119] data portal (https://www.eqtlgen.org) on April 15 2022. No *trans*-eQTL passed the arbitrary significance threshold (Bonferroni *P* value <0.05) for association with *C5*. 1921 single nucleotide variants (SNVs) were identified as C5 cis-eQTL using the same threshold. These were visualized using the Integrative Genomics Viewer v 2.12.2 (Broad Institute) [120]. Highly significant C5 cis-eQTL (Bonferroni *P* value $<10^{-100}$) were subjected to Linkage disequilibrium (LD) analysis and visualization using Haploview 4.2 (Broad Institute) [121] by the default algorithm of Gabriel et al. [122], which identified ten strong LD blocks. GBR (1000 genomes) was used as the reference population for LD analysis as it was the closest population to the patients in our study.

Analysis of the sourced transcriptome data—For analysis of the transcriptional signature during candidemia in humans, transcriptional data from whole blood of healthy human volunteers and patients with candidemia were sourced from the GEO database (GSE176262); these data were acquired using RNA from whole blood, collected in PAXgene tubes at the time of first culture positivity for *Candida* species [17]. To determine the transcriptional response of human PBMC after *ex vivo* stimulation with different fungi, we sourced a previously published transcriptional dataset [20] deposited under the accession code GSE162746. For defining the host RNA-seq signature in kidneys before and after infection, we sourced data from temporal transcriptional data available at the GEO database, under the accession code GSE56092 [29]. The sourced data were mapped with Bowtie 2 [123] and aligned using Rsubread [124]. Subsequently, RPKM and differential expression were determined using edgeR [125]. To define differentially enriched pathways in candidemic patients or human PBMC post-fungal stimulation or mouse kidneys post-infection, we used pre-ranked GSEA [18] and the pathways curated in MSigDB [19]. Significantly enriched pathways are shown in Table S1A (candidemic patients' data) and Table S2 (mouse kidney data).

QUANTIFICATION AND STATISTICAL ANALYSIS

For assessing statistical significance between groups, unpaired t tests (with or without Welch's correction), paired t test, Mann-Whitney U tests, Ordinary one-way ANOVA or Kruskal-Wallis tests with Tukey's or Dunn's multiple comparison tests, log-rank test,

2-way ANOVA with Holm-Sidak's or Dunnette's multiple comparisons tests, and Fisher's exact test were used, where appropriate. GraphPad Prism 8 and R were used for these analyses. For transcriptional profiling FDR < 0.01 was considered statistically significant. A *P* value less than 0.05 was considered statistically significant for differences in grouped comparisons.

Supplementary Material

Refer to Web version on PubMed Central for supplementary material.

Acknowledgements

This work was supported by the DIR of NIAID, NIDDK, NHLBI, NIDCR, and NINDS (IRP support; LND) and grants from NIAID (R00AI141622; JVD), NIGMS (R35GM138283; MK), NIDCR (1K99DE030124–01A1; LMS), University of Toledo (de Arce-Koch Memorial Endowment Fund; HC), ERC Grant (#833247; MGN), German Research Foundation (FR 3851/2–1; TF), and Spinoza Grant of the Netherlands Organization for Scientific Research (MGN). LND and EB were supported by the Departamento de Histología y Embriología, Universidad de la República, Uruguay and the NIH Oxford-Cambridge Scholars Program, respectively. We thank the NIAID animal facilities and research technology branch.

References

1. Bongomin F, Gago S, Oladele R, and Denning D (2017). Global and Multi-National Prevalence of Fungal Diseases—Estimate Precision. Journal of Fungi 3, 57. [PubMed: 29371573]
2. Pappas PG, Lionakis MS, Arendrup MC, Ostrosky-Zeichner L, and Kullberg BJ (2018). Invasive candidiasis. Nat Rev Dis Primers 4, 18026. 10.1038/nrdp.2018.26. [PubMed: 29749387]
3. Socié G, Caby-Tosi M-P, Marantz JL, Cole A, Bedrosian CL, Gasteyger C, Mujeebuddin A, Hillmen P, Vande Walle J, and Haller H (2019). Eculizumab in paroxysmal nocturnal haemoglobinuria and atypical haemolytic uraemic syndrome: 10-year pharmacovigilance analysis. British Journal of Haematology 185, 297–310. 10.1111/bjh.15790. [PubMed: 30768680]
4. Jodele S, Dandoy CE, Lane A, Laskin BL, Teusink-Cross A, Myers KC, Wallace G, Nelson A, Bleesing J, Chima RS, et al. (2020). Complement blockade for TA-TMA: lessons learned from a large pediatric cohort treated with eculizumab. Blood 135, 1049–1057. 10.1182/blood.2019004218. [PubMed: 31932840]
5. Federal-Drug-Administration. Eculizumab FDA label (https://www.accessdata.fda.gov/spl/data/68907414-19b7-43c7-be48-9768bb97d696/68907414-19b7-43c7-be48-9768bb97d696.xml#S5.1).
6. Lionakis MS, Iliev ID, and Hohl TM (2017). Immunity against fungi. JCI Insight 2. 10.1172/jci.insight.93156.
7. Lionakis MS, Drummond RA, and Hohl TM (2023). Immune responses to human fungal pathogens and therapeutic prospects. Nat Rev Immunol, 1–20. 10.1038/s41577-022-00826-w.
8. Hess C, and Kemper C (2016). Complement-Mediated Regulation of Metabolism and Basic Cellular Processes. Immunity 45, 240–254. 10.1016/j.immuni.2016.08.003. [PubMed: 27533012]
9. Hajishengallis G, Reis ES, Mastellos DC, Ricklin D, and Lambris JD (2017). Novel mechanisms and functions of complement. Nature Immunology 18, 1288–1298. 10.1038/ni.3858. [PubMed: 29144501]
10. Rosenfeld SI, Kelly ME, and Leddy JP (1976). Hereditary deficiency of the fifth component of complement in man. I. Clinical, immunochemical, and family studies. J Clin Invest 57, 1626–1634. 10.1172/JCI108433. [PubMed: 932197]
11. Ricklin D, and Lambris JD (2013). Complement in immune and inflammatory disorders: pathophysiological mechanisms. J Immunol 190, 3831–3838. 10.4049/jimmunol.1203487. [PubMed: 23564577]
12. Yan B, Freiwald T, Chauss D, Wang L, West E, Mirabelli C, Zhang CJ, Nichols EM, Malik N, Gregory R, et al. (2021). SARS-CoV-2 drives JAK1/2-dependent local complement hyperactivation. Sci Immunol 6. 10.1126/sciimmunol.abg0833.

13. Mastellos DC, Ricklin D, and Lambris JD (2019). Clinical promise of next-generation complement therapeutics. Nature Reviews Drug Discovery 18, 707–729. 10.1038/s41573-019-0031-6. [PubMed: 31324874]

14. Reis ES, Mastellos DC, Hajishengallis G, and Lambris JD (2019). New insights into the immune functions of complement. Nat Rev Immunol 19, 503–516. 10.1038/s41577-019-0168-x. [PubMed: 31048789]

15. Niyonzima N, Rahman J, Kunz N, West EE, Freiwald T, Desai JV, Merle NS, Gidon A, Sporsheim B, Lionakis MS, et al. (2021). Mitochondrial C5aR1 activity in macrophages controls IL-1beta production underlying sterile inflammation. Sci Immunol 6, eabf2489. 10.1126/sciimmunol.abf2489. [PubMed: 34932384]

16. Arbore G, West EE, Spolski R, Robertson AAB, Klos A, Rheinheimer C, Dutow P, Woodruff TM, Yu ZX, O'Neill LA, et al. (2016). T helper 1 immunity requires complement-driven NLRP3 inflammasome activity in CD4(+) T cells. Science 352, aad1210. 10.1126/science.aad1210. [PubMed: 27313051]

17. Steinbrink JM, Myers RA, Hua K, Johnson MD, Seidelman JL, Tsalik EL, Henao R, Ginsburg GS, Woods CW, Alexander BD, and McClain MT (2021). The host transcriptional response to Candidemia is dominated by neutrophil activation and heme biosynthesis and supports novel diagnostic approaches. Genome Medicine 13, 108. 10.1186/s13073-021-00924-9. [PubMed: 34225776]

18. Subramanian A, Tamayo P, Mootha VK, Mukherjee S, Ebert BL, Gillette MA, Paulovich A, Pomeroy SL, Golub TR, Lander ES, and Mesirov JP (2005). Gene set enrichment analysis: a knowledge-based approach for interpreting genome-wide expression profiles. Proc Natl Acad Sci U S A 102, 15545–15550. 10.1073/pnas.0506580102. [PubMed: 16199517]

19. Liberzon A, Birger C, Thorvaldsdottir H, Ghandi M, Mesirov JP, and Tamayo P (2015). The Molecular Signatures Database (MSigDB) hallmark gene set collection. Cell Syst 1, 417–425. 10.1016/j.cels.2015.12.004. [PubMed: 26771021]

20. Bruno M, Dewi IMW, Matzaraki V, Ter Horst R, Pekmezovic M, Rosler B, Groh L, Roring RJ, Kumar V, Li Y, et al. (2021). Comparative host transcriptome in response to pathogenic fungi identifies common and species-specific transcriptional antifungal host response pathways. Comput Struct Biotechnol J 19, 647–663. 10.1016/j.csbj.2020.12.036. [PubMed: 33510868]

21. Spellberg B, Ibrahim AS, Edwards JE Jr., and Filler SG (2005). Mice with disseminated candidiasis die of progressive sepsis. J Infect Dis 192, 336–343. 10.1086/430952. [PubMed: 15962230]

22. Lionakis MS, Lim JK, Lee CC, and Murphy PM (2011). Organ-specific innate immune responses in a mouse model of invasive candidiasis. J Innate Immun 3, 180–199. 10.1159/000321157. [PubMed: 21063074]

23. Ashman RB, Bolitho EM, and Papadimitriou JM (1993). Patterns of resistance to Candida albicans in inbred mouse strains. Immunol Cell Biol 71 (Pt 3), 221–225. 10.1038/icb.1993.25. [PubMed: 8349305]

24. Mullick A, Leon Z, Min-Oo G, Berghout J, Lo R, Daniels E, and Gros P (2006). Cardiac failure in C5-deficient A/J mice after Candida albicans infection. Infect Immun 74, 4439–4451. 10.1128/IAI.00159-06. [PubMed: 16861630]

25. Mullick A, Elias M, Picard S, Bourget L, Jovcevski O, Gauthier S, Tuite A, Harakidas P, Bihun C, Massie B, and Gros P (2004). Dysregulated inflammatory response to Candida albicans in a C5-deficient mouse strain. Infect Immun 72, 5868–5876. 10.1128/IAI.72.10.5868-5876.2004. [PubMed: 15385488]

26. Mullick A, Tremblay J, Leon Z, and Gros P (2011). A novel role for the fifth component of complement (C5) in cardiac physiology. PLoS One 6, e22919. 10.1371/journal.pone.0022919. [PubMed: 21829669]

27. Diez E, Lee SH, Gauthier S, Yaraghi Z, Tremblay M, Vidal S, and Gros P (2003). Birc1e is the gene within the Lgn1 locus associated with resistance to Legionella pneumophila. Nat Genet 33, 55–60. 10.1038/ng1065. [PubMed: 12483212]

28. Mitsos LM, Cardon LR, Ryan L, LaCourse R, North RJ, and Gros P (2003). Susceptibility to tuberculosis: a locus on mouse chromosome 19 (Trl-4) regulates Mycobacterium tuberculosis

replication in the lungs. Proc Natl Acad Sci U S A 100, 6610–6615. 10.1073/pnas.1031727100. [PubMed: 12740444]

29. Liu YP, Shetty AC, Schwartz JA, Bradford LL, Xu WJ, Phan QT, Kumari P, Mahurkar A, Mitchell AP, Ravel J, et al. (2015). New signaling pathways govern the host response to C. albicans infection in various niches. Genome Res 25, 679–689. 10.1101/gr.187427.114. [PubMed: 25858952]
30. Lionakis MS, and Levitz SM (2018). Host Control of Fungal Infections: Lessons from Basic Studies and Human Cohorts. Annu Rev Immunol 36, 157–191. 10.1146/annurev-immunol-042617-053318. [PubMed: 29237128]
31. Karsten CM, Laumonnier Y, Eurich B, Ender F, Broker K, Roy S, Czabanska A, Vollbrandt T, Figge J, and Kohl J (2015). Monitoring and cell-specific deletion of C5aR1 using a novel floxed GFP-C5aR1 reporter knock-in mouse. J Immunol 194, 1841–1855. 10.4049/jimmunol.1401401. [PubMed: 25589074]
32. Fayyazi A, Scheel O, Werfel T, Schweyer S, Oppermann M, Gotze O, Radzun HJ, and Zwirner J (2000). The C5a receptor is expressed in normal renal proximal tubular but not in normal pulmonary or hepatic epithelial cells. Immunology 99, 38–45. [PubMed: 10651939]
33. Zahedi R, Braun M, Wetsel RA, Ault BH, Khan A, Welch TR, Frenzke M, and Davis AE (2000). The C5a receptor is expressed by human renal proximal tubular epithelial cells. Clin Exp Immunol 121, 226–233. [PubMed: 10931135]
34. Sahu RK, Xavier S, Chauss D, Wang L, Chew C, Taylor R, Stallcup WB, Ma JZ, Kazemian M, Afzali B, et al. (2022). Folic acid-mediated fibrosis is driven by C5a receptor 1-mediated activation of kidney myeloid cells. Am J Physiol Renal Physiol 322, F597–F610. 10.1152/ajprenal.00404.2021. [PubMed: 35379003]
35. Lopes JP, and Lionakis MS (2022). Pathogenesis and virulence of Candida albicans. Virulence 13, 89–121. 10.1080/21505594.2021.2019950. [PubMed: 34964702]
36. Passegue E, Wagner EF, and Weissman IL (2004). JunB deficiency leads to a myeloproliferative disorder arising from hematopoietic stem cells. Cell 119, 431–443. 10.1016/j.cell.2004.10.010. [PubMed: 15507213]
37. Yona S, Kim KW, Wolf Y, Mildner A, Varol D, Breker M, Strauss-Ayali D, Viukov S, Guilliams M, Misharin A, et al. (2013). Fate mapping reveals origins and dynamics of monocytes and tissue macrophages under homeostasis. Immunity 38, 79–91. 10.1016/j.immuni.2012.12.001. [PubMed: 23273845]
38. Clausen BE, Burkhardt C, Reith W, Renkawitz R, and Forster I (1999). Conditional gene targeting in macrophages and granulocytes using LysMcre mice. Transgenic Res 8, 265–277. 10.1023/a:1008942828960. [PubMed: 10621974]
39. Miyabe Y, Miyabe C, Murooka TT, Kim EY, Newton GA, Kim ND, Haribabu B, Luscinskas FW, Mempel TR, and Luster AD (2017). Complement C5a Receptor is the Key Initiator of Neutrophil Adhesion Igniting Immune Complex-induced Arthritis. Sci Immunol 2. 10.1126/sciimmunol.aaj2195.
40. Engelke C, Wiese AV, Schmudde I, Ender F, Strover HA, Vollbrandt T, Konig P, Laumonnier Y, and Kohl J (2014). Distinct roles of the anaphylatoxins C3a and C5a in dendritic cell-mediated allergic asthma. J Immunol 193, 5387–5401. 10.4049/jimmunol.1400080. [PubMed: 25355927]
41. Chou RC, Kim ND, Sadik CD, Seung E, Lan Y, Byrne MH, Haribabu B, Iwakura Y, and Luster AD (2010). Lipid-cytokine-chemokine cascade drives neutrophil recruitment in a murine model of inflammatory arthritis. Immunity 33, 266–278. 10.1016/j.immuni.2010.07.018. [PubMed: 20727790]
42. Bohnsack JF, Widjaja K, Ghazizadeh S, Rubens CE, Hillyard DR, Parker CJ, Albertine KH, and Hill HR (1997). A role for C5 and C5a-ase in the acute neutrophil response to group B streptococcal infections. J Infect Dis 175, 847–855. 10.1086/513981. [PubMed: 9086140]
43. Briukhovetska D, Ohm B, Mey FT, Aliberti J, Kleingarn M, Huber-Lang M, Karsten CM, and Kohl J (2020). C5aR1 Activation Drives Early IFN-gamma Production to Control Experimental Toxoplasma gondii Infection. Front Immunol 11, 1397. 10.3389/fimmu.2020.01397. [PubMed: 32733463]

44. Toews GB, and Vial WC (1984). The role of C5 in polymorphonuclear leukocyte recruitment in response to Streptococcus pneumoniae. Am Rev Respir Dis 129, 82–86. 10.1164/arrd.1984.129.1.82. [PubMed: 6703488]
45. Prat-Luri B, Neal C, Passelli K, Ganga E, Amore J, Firmino-Cruz L, Petrova TV, Muller AJ, and Tacchini-Cottier F (2022). The C5a-C5aR1 complement axis is essential for neutrophil recruitment to draining lymph nodes via high endothelial venules in cutaneous leishmaniasis. Cell Rep 39, 110777. 10.1016/j.celrep.2022.110777. [PubMed: 35508133]
46. Lionakis MS, Swamydas M, Fischer BG, Plantinga TS, Johnson MD, Jaeger M, Green NM, Masedunskas A, Weigert R, Mikelis C, et al. (2013). CX3CR1-dependent renal macrophage survival promotes Candida control and host survival. J Clin Invest 123, 5035–5051. 10.1172/JCI71307. [PubMed: 24177428]
47. Swamydas M, Gao JL, Break TJ, Johnson MD, Jaeger M, Rodriguez CA, Lim JK, Green NM, Collar AL, Fischer BG, et al. (2016). CXCR1-mediated neutrophil degranulation and fungal killing promote Candida clearance and host survival. Sci Transl Med 8, 322ra310. 10.1126/scitranslmed.aac7718.
48. Dominguez-Andres J, Feo-Lucas L, Minguito de la Escalera, M., Gonzalez, L., Lopez-Bravo, M., and Ardavin, C. (2017). Inflammatory Ly6Chigh Monocytes Protect against Candidiasis through IL-15-Driven NK Cell/Neutrophil Activation. Immunity 46, 1059–1072 e1054. 10.1016/j.immuni.2017.05.009. [PubMed: 28636955]
49. Whitney PG, Bar E, Osorio F, Rogers NC, Schraml BU, Deddouche S, LeibundGut-Landmann S, and Reis e Sousa C (2014). Syk signaling in dendritic cells orchestrates innate resistance to systemic fungal infection. PLoS Pathog 10, e1004276. 10.1371/journal.ppat.1004276. [PubMed: 25033445]
50. Marino MW, Dunn A, Grail D, Inglese M, Noguchi Y, Richards E, Jungbluth A, Wada H, Moore M, Williamson B, et al. (1997). Characterization of tumor necrosis factor-deficient mice. Proc Natl Acad Sci U S A 94, 8093–8098. 10.1073/pnas.94.15.8093. [PubMed: 9223320]
51. van Enckevort FH, Netea MG, Hermus AR, Sweep CG, Meis JF, Van der Meer JW, and Kullberg BJ (1999). Increased susceptibility to systemic candidiasis in interleukin-6 deficient mice. Med Mycol 37, 419–426. 10.1046/j.1365-280x.1999.00247.x. [PubMed: 10647123]
52. Vonk AG, Netea MG, van Krieken JH, Iwakura Y, van der Meer JW, and Kullberg BJ (2006). Endogenous interleukin (IL)-1 alpha and IL-1 beta are crucial for host defense against disseminated candidiasis. J Infect Dis 193, 1419–1426. 10.1086/503363. [PubMed: 16619190]
53. Qian Q, Jutila MA, Van Rooijen N, and Cutler JE (1994). Elimination of mouse splenic macrophages correlates with increased susceptibility to experimental disseminated candidiasis. J Immunol 152, 5000–5008. [PubMed: 8176217]
54. Teo YJ, Ng SL, Mak KW, Setiagani YA, Chen Q, Nair SK, Sheng J, and Ruedl C (2021). Renal CD169(++) resident macrophages are crucial for protection against acute systemic candidiasis. Life Sci Alliance 4. 10.26508/lsa.202000890.
55. Lalli PN, Strainic MG, Yang M, Lin F, Medof ME, and Heeger PS (2008). Locally produced C5a binds to T cell–expressed C5aR to enhance effector T-cell expansion by limiting antigen-induced apoptosis. Blood 112, 1759–1766. 10.1182/blood-2008-04-151068. [PubMed: 18567839]
56. Kasper L, König A, Koenig P-A, Gresnigt MS, Westman J, Drummond RA, Lionakis MS, Groß O, Ruland J, Naglik JR, and Hube B (2018). The fungal peptide toxin Candidalysin activates the NLRP3 inflammasome and causes cytolysis in mononuclear phagocytes. Nature Communications 9, 4260. 10.1038/s41467-018-06607-1.
57. Cao M, Wu Z, Lou Q, Lu W, Zhang J, Li Q, Zhang Y, Yao Y, Zhao Q, Li M, et al. (2019). Dectin-1-induced RIPK1 and RIPK3 activation protects host against Candida albicans infection. Cell Death Differ 26, 2622–2636. 10.1038/s41418-019-0323-8. [PubMed: 30944411]
58. Wellington M, Koselny K, Sutterwala FS, and Krysan DJ (2014). Candida albicans triggers NLRP3-mediated pyroptosis in macrophages. Eukaryot Cell 13, 329–340. 10.1128/EC.00336-13. [PubMed: 24376002]
59. Millet N, Solis NV, Aguilar D, Lionakis MS, Wheeler RT, Jendzjowsky N, and Swidergall M (2021). IL-23 signaling prevents ferroptosis-driven renal immunopathology during candidiasis. bioRxiv, 2021.2012.2019.473386. 10.1101/2021.12.19.473386.

60. Klos A, Tenner AJ, Johswich KO, Ager RR, Reis ES, and Kohl J (2009). The role of the anaphylatoxins in health and disease. Mol Immunol 46, 2753–2766. 10.1016/j.molimm.2009.04.027. [PubMed: 19477527]
61. Collar AL, Swamydas M, O'Hayre M, Sajib MS, Hoffman KW, Singh SP, Mourad A, Johnson MD, Ferre EM, Farber JM, et al. (2018). The homozygous CX3CR1-M280 mutation impairs human monocyte survival. JCI Insight 3. 10.1172/jci.insight.95417.
62. Brown GD (2011). Innate antifungal immunity: the key role of phagocytes. Annu Rev Immunol 29, 1–21. 10.1146/annurev-immunol-030409-101229. [PubMed: 20936972]
63. Desai JV (2018). Candida albicans Hyphae: From Growth Initiation to Invasion. J Fungi (Basel) 4. 10.3390/jof4010010.
64. Jhingran A, Mar KB, Kumasaka DK, Knoblaugh SE, Ngo LY, Segal BH, Iwakura Y, Lowell CA, Hamerman JA, Lin X, and Hohl TM (2012). Tracing conidial fate and measuring host cell antifungal activity using a reporter of microbial viability in the lung. Cell Rep 2, 1762–1773. 10.1016/j.celrep.2012.10.026. [PubMed: 23200858]
65. Heung LJ, Jhingran A, and Hohl TM (2015). Deploying FLAREs to Visualize Functional Outcomes of Host-Pathogen Encounters. PLoS Pathog 11, e1004912. 10.1371/journal.ppat.1004912. [PubMed: 26158781]
66. Jawale CV, Ramani K, Li D. d., Coleman BM, Oberoi RS, Kupul S, Lin L, Desai JV, Delgoffe GM, Lionakis MS, et al. (2020). Restoring glucose uptake rescues neutrophil dysfunction and protects against systemic fungal infection in mouse models of kidney disease. Science Translational Medicine 12, eaay5691. doi:10.1126/scitranslmed.aay5691. [PubMed: 32554707]
67. Li DD, Jawale CV, Zhou C, Lin L, Trevejo-Nunez GJ, Rahman SA, Mullet SJ, Das J, Wendell SG, Delgoffe GM, et al. (2022). Fungal sensing enhances neutrophil metabolic fitness by regulating antifungal Glut1 activity. Cell Host Microbe 30, 530–544 e536. 10.1016/j.chom.2022.02.017. [PubMed: 35316647]
68. Jayne DRW, Merkel PA, Schall TJ, and Bekker P (2021). Avacopan for the Treatment of ANCA-Associated Vasculitis. New England Journal of Medicine 384, 599–609. 10.1056/NEJMoa2023386. [PubMed: 33596356]
69. Tsoni SV, Kerrigan Ann M, Marakalala Mohlopheni J, Srinivasan N, Duffield M, Taylor Philip R, Botto M, Steele C, and Brown Gordon D (2009). Complement C3 Plays an Essential Role in the Control of Opportunistic Fungal Infections. Infection and Immunity 77, 3679–3685. 10.1128/IAI.00233-09. [PubMed: 19581397]
70. Weichhart T, Hengstschlager M, and Linke M (2015). Regulation of innate immune cell function by mTOR. Nature Reviews Immunology 15, 599–614. 10.1038/nri3901.
71. Zhang X, Sergin I, Evans TD, Jeong SJ, Rodriguez-Velez A, Kapoor D, Chen S, Song E, Holloway KB, Crowley JR, et al. (2020). High-protein diets increase cardiovascular risk by activating macrophage mTOR to suppress mitophagy. Nat Metab 2, 110–125. 10.1038/s42255-019-0162-4. [PubMed: 32128508]
72. Kato H, Nakajima S, Saito Y, Takahashi S, Katoh R, and Kitamura M (2012). mTORC1 serves ER stress-triggered apoptosis via selective activation of the IRE1-JNK pathway. Cell Death Differ 19, 310–320. 10.1038/cdd.2011.98. [PubMed: 21779001]
73. He L, Weber KJ, Diwan A, and Schilling JD (2016). Inhibition of mTOR reduces lipotoxic cell death in primary macrophages through an autophagy-independent mechanism. J Leukocyte Biol 100, 1113–1124. 10.1189/jlb.3A1015-463R. [PubMed: 27312848]
74. Cruz MC, Goldstein AL, Blankenship J, Del Poeta M, Perfect JR, McCusker JH, Bennani YL, Cardenas ME, and Heitman J (2001). Rapamycin and less immunosuppressive analogs are toxic to Candida albicans and Cryptococcus neoformans via FKBP12-dependent inhibition of TOR. Antimicrob Agents Chemother 45, 3162–3170. 10.1128/AAC.45.11.3162-3170.2001. [PubMed: 11600372]
75. Morgan BP, and Gasque P (1997). Extrahepatic complement biosynthesis: where, when and why? Clin Exp Immunol 107, 1–7. 10.1046/j.1365-2249.1997.d01-890.x. [PubMed: 9010248]
76. Freeley S, Kemper C, and Le Friec G (2016). The "ins and outs" of complement-driven immune responses. Immunological Reviews 274, 16–32. 10.1111/imr.12472. [PubMed: 27782335]

77. Võsa U, Claringbould A, Westra H-J, Bonder MJ, Deelen P, Zeng B, Kirsten H, Saha A, Kreuzhuber R, Yazar S, et al. (2021). Large-scale cis- and trans-eQTL analyses identify thousands of genetic loci and polygenic scores that regulate blood gene expression. Nature Genetics 53, 1300–1310. 10.1038/s41588-021-00913-z. [PubMed: 34475573]

78. Xu D, Yi H, Yu S, Li X, Qiao Y, and Deng W (2016). Association of Complement C5 Gene Polymorphisms with Proliferative Diabetic Retinopathy of Type 2 Diabetes in a Chinese Han Population. PLOS ONE 11, e0149704. 10.1371/journal.pone.0149704. [PubMed: 26934706]

79. Xu D, Hou S, Jiang Y, Zhang J, Cao S, Zhang D, Luo L, Kijlstra A, and Yang P (2015). Complement C5 Gene Confers Risk for Acute Anterior Uveitis. Investigative Ophthalmology & Visual Science 56, 4954–4960. 10.1167/iovs.15-16645. [PubMed: 26230759]

80. Lausen B SM (1992). Maximally selected rank statistics. Biometrics 48, 73–85.

81. Hothorn T LB (2003). On the exact distribution of maximally selected rank statistics. Computational Statistics & Data Analysis 43, 121–137.

82. Delgado J, Pereira A, Villamor N, Lopez-Guillermo A, and Rozman C (2014). Survival analysis in hematologic malignancies: recommendations for clinicians. Haematologica 99, 1410–1420. 10.3324/haematol.2013.100784. [PubMed: 25176982]

83. Romani L, Mencacci A, Cenci E, Del Sero G, Bistoni F, and Puccetti P (1997). An immunoregulatory role for neutrophils in CD4+ T helper subset selection in mice with candidiasis. J Immunol 158, 2356–2362. [PubMed: 9036985]

84. Hunniger K, Bieber K, Martin R, Lehnert T, Figge MT, Loffler J, Guo RF, Riedemann NC, and Kurzai O (2015). A Second Stimulus Required for Enhanced Antifungal Activity of Human Neutrophils in Blood Is Provided by Anaphylatoxin C5a. Journal of Immunology 194, 1199–1210. 10.4049/jimmunol.1401845.

85. Lee EKS, Gillrie MR, Li L, Arnason JW, Kim JH, Babes L, Lou Y, Sanati-Nezhad A, Kyei SK, Kelly MM, et al. (2018). Leukotriene B4-Mediated Neutrophil Recruitment Causes Pulmonary Capillaritis during Lethal Fungal Sepsis. Cell Host Microbe 23, 121–133 e124. 10.1016/j.chom.2017.11.009. [PubMed: 29290576]

86. Shushakova N, Skokowa J, Schulman J, Baumann U, Zwirner J, Schmidt RE, and Gessner JE (2002). C5a anaphylatoxin is a major regulator of activating versus inhibitory FcgammaRs in immune complex-induced lung disease. J Clin Invest 110, 1823–1830. 10.1172/JCI16577. [PubMed: 12488432]

87. Kumar V, Ali SR, Konrad S, Zwirner J, Verbeek JS, Schmidt RE, and Gessner JE (2006). Cell-derived anaphylatoxins as key mediators of antibody-dependent type II autoimmunity in mice. J Clin Invest 116, 512–520. 10.1172/JCI25536. [PubMed: 16453025]

88. Godau J, Heller T, Hawlisch H, Trappe M, Howells E, Best J, Zwirner J, Verbeek JS, Hogarth PM, Gerard C, et al. (2004). C5a initiates the inflammatory cascade in immune complex peritonitis. J Immunol 173, 3437–3445. 10.4049/jimmunol.173.5.3437. [PubMed: 15322209]

89. Karsten CM, Pandey MK, Figge J, Kilchenstein R, Taylor PR, Rosas M, McDonald JU, Orr SJ, Berger M, Petzold D, et al. (2012). Anti-inflammatory activity of IgG1 mediated by Fc galactosylation and association of FcgammaRIIB and dectin-1. Nat Med 18, 1401–1406. 10.1038/nm.2862. [PubMed: 22922409]

90. Friscic J, Bottcher M, Reinwald C, Bruns H, Wirth B, Popp SJ, Walker KI, Ackermann JA, Chen X, Turner J, et al. (2021). The complement system drives local inflammatory tissue priming by metabolic reprogramming of synovial fibroblasts. Immunity 54, 1002–1021 e1010. 10.1016/j.immuni.2021.03.003. [PubMed: 33761330]

91. Kolev M, Dimeloe S, Le Friec G, Navarini A, Arbore G, Povoleri GA, Fischer M, Belle R, Loeliger J, Develioglu L, et al. (2015). Complement Regulates Nutrient Influx and Metabolic Reprogramming during Th1 Cell Responses. Immunity 42, 1033–1047. 10.1016/j.immuni.2015.05.024. [PubMed: 26084023]

92. Evavold CL, Hafner-Bratkovic I, Devant P, D'Andrea JM, Ngwa EM, Borsic E, Doench JG, LaFleur MW, Sharpe AH, Thiagarajah JR, and Kagan JC (2021). Control of gasdermin D oligomerization and pyroptosis by the Ragulator-Rag-mTORC1 pathway. Cell 184, 4495–4511 e4419. 10.1016/j.cell.2021.06.028. [PubMed: 34289345]

93. Li T, Xie Y, Shi L, Sun Y, Wen J, Deng Z, Zhang H, Li H, Yang J, and Xiao H (2021). TSC1 Suppresses Macrophage Necroptosis for the Control of Infection by Fungal Pathogen Candida albicans. ImmunoHorizons 5, 90–101. 10.4049/immunohorizons.2000093. [PubMed: 33597177]

94. Kim EY, Ner-Gaon H, Varon J, Cullen AM, Guo J, Choi J, Barragan-Bradford D, Higuera A, Pinilla-Vera M, Short SAP, et al. (2020). Post-sepsis immunosuppression depends on NKT cell regulation of mTOR/IFN-γ in NK cells. The Journal of Clinical Investigation 130, 3238–3252. 10.1172/JCI128075. [PubMed: 32154791]

95. Cheng SC, Quintin J, Cramer RA, Shepardson KM, Saeed S, Kumar V, Giamarellos-Bourboulis EJ, Martens JH, Rao NA, Aghajanirefah A, et al. (2014). mTOR- and HIF-1alpha-mediated aerobic glycolysis as metabolic basis for trained immunity. Science 345, 1250684. 10.1126/science.1250684. [PubMed: 25258083]

96. Huber-Lang M, Younkin EM, Sarma JV, Riedemann N, McGuire SR, Lu KT, Kunkel R, Younger JG, Zetoune FS, and Ward PA (2002). Generation of C5a by Phagocytic Cells. The American Journal of Pathology 161, 1849–1859. 10.1016/S0002-9440(10)64461-6. [PubMed: 12414531]

97. West EE, Kolev M, and Kemper C (2018). Complement and the Regulation of T Cell Responses. Annual Review of Immunology 36, 309–338. 10.1146/annurev-immunol-042617-053245.

98. Sahu SK, Ozanturk AN, Kulkarni DH, Ma L, Barve RA, Dannull L, Lu A, Starick M, McPhatter J, Garnica L, et al. (2023). Lung epithelial cell-derived C3 protects against pneumonia-induced lung injury. Sci Immunol 8, eabp9547. 10.1126/sciimmunol.abp9547. [PubMed: 36735773]

99. Georg P, Astaburuaga-Garcia R, Bonaguro L, Brumhard S, Michalick L, Lippert LJ, Kostevc T, Gabel C, Schneider M, Streitz M, et al. (2022). Complement activation induces excessive T cell cytotoxicity in severe COVID-19. Cell 185, 493–512 e425. 10.1016/j.cell.2021.12.040. [PubMed: 35032429]

100. Verschoor A, Brockman MA, Knipe DM, and Carroll MC (2001). Cutting edge: myeloid complement C3 enhances the humoral response to peripheral viral infection. J Immunol 167, 2446–2451. 10.4049/jimmunol.167.5.2446. [PubMed: 11509581]

101. Kiss Máté G., N.P.-M., Porsch Florentina, Tsiantoulas Dimitrios, Hendrikx Tim, Takaoka Minoru, Dinh Huy Q., Narzt Marie-Sophie, Göderle Laura, Ozsvár-Kozma Mária, Schuster Michael, Fortelny Nikolaus, Hladik Anastasiya, Knapp Sylvia, Gruber Florian, Pickering7 Matthew C., Bock2 Christoph, Swirski Filip K., Ley Klaus, Zernecke Alma, Cochain Clément, Kemper Claudia, Mallat Ziad, Binder Christoph J. (2023). On-site complement factor H production limits efferocytosis and exacerbates atherosclerosis. Immunity.

102. Ding P, Xu Y, Li L, Lv X, Li L, Chen J, Zhou D, Wang X, Wang Q, Zhang W, et al. (2022). Intracellular complement C5a/C5aR1 stabilizes beta-catenin to promote colorectal tumorigenesis. Cell Rep 39, 110851. 10.1016/j.celrep.2022.110851. [PubMed: 35649359]

103. Yang MM, Wang J, Ren H, Sun YD, Fan JJ, Teng Y, and Li YB (2016). Genetic Investigation of Complement Pathway Genes in Type 2 Diabetic Retinopathy: An Inflammatory Perspective. Mediators of Inflammation 2016, 1313027. 10.1155/2016/1313027. [PubMed: 26989329]

104. European-Medicines-Agency pegcetacoplan EMA label (https://www.ema.europa.eu/en/documents/product-information/aspaveli-epar-product-information_en.pdf).

105. Federal-Drug-Administration. pegcetacoplan FDA label (https://www.accessdata.fda.gov/drugsatfda_docs/label/2021/215014s000lbl.pdf).

106. Syed SN, Konrad S, Wiege K, Nieswandt B, Nimmerjahn F, Schmidt RE, and Gessner JE (2009). Both FcgammaRIV and FcgammaRIII are essential receptors mediating type II and type III autoimmune responses via FcRgamma-LAT-dependent generation of C5a. Eur J Immunol 39, 3343–3356. 10.1002/eji.200939884. [PubMed: 19795417]

107. Brown GD, Willment JA, and Whitehead L (2018). C-type lectins in immunity and homeostasis. Nature Reviews Immunology 18, 374–389. 10.1038/s41577-018-0004-8.

108. Gerard NP, Lu B, Liu P, Craig S, Fujiwara Y, Okinaga S, and Gerard C (2005). An anti-inflammatory function for the complement anaphylatoxin C5a-binding protein, C5L2. J Biol Chem 280, 39677–39680. 10.1074/jbc.C500287200. [PubMed: 16204243]

109. Kolev M, West EE, Kunz N, Chauss D, Moseman EA, Rahman J, Freiwald T, Balmer ML, Lotscher J, Dimeloe S, et al. (2020). Diapedesis-Induced Integrin Signaling via LFA-1 Facilitates

Tissue Immunity by Inducing Intrinsic Complement C3 Expression in Immune Cells. Immunity 52, 513–527 e518. 10.1016/j.immuni.2020.02.006. [PubMed: 32187519]

110. Yano J, and Fidel PL Jr. (2011). Protocols for vaginal inoculation and sample collection in the experimental mouse model of Candida vaginitis. J Vis Exp. 10.3791/3382.
111. Break TJ, Oikonomou V, Dutzan N, Desai JV, Swidergall M, Freiwald T, Chauss D, Harrison OJ, Alejo J, Williams DW, et al. (2021). Aberrant type 1 immunity drives susceptibility to mucosal fungal infections. Science 371. 10.1126/science.aay5731.
112. Brothers KM, Gratacap RL, Barker SE, Newman ZR, Norum A, and Wheeler RT (2013). NADPH oxidase-driven phagocyte recruitment controls Candida albicans filamentous growth and prevents mortality. PLoS Pathog 9, e1003634. 10.1371/journal.ppat.1003634. [PubMed: 24098114]
113. Dobin A, Davis CA, Schlesinger F, Drenkow J, Zaleski C, Jha S, Batut P, Chaisson M, and Gingeras TR (2013). STAR: ultrafast universal RNA-seq aligner. Bioinformatics 29, 15–21. 10.1093/bioinformatics/bts635. [PubMed: 23104886]
114. Ritchie ME, Phipson B, Wu D, Hu Y, Law CW, Shi W, and Smyth GK (2015). limma powers differential expression analyses for RNA-sequencing and microarray studies. Nucleic Acids Res 43, e47. 10.1093/nar/gkv007. [PubMed: 25605792]
115. Schindelin J, Arganda-Carreras I, Frise E, Kaynig V, Longair M, Pietzsch T, Preibisch S, Rueden C, Saalfeld S, Schmid B, et al. (2012). Fiji: an open-source platform for biological-image analysis. Nat Methods 9, 676–682. 10.1038/nmeth.2019. [PubMed: 22743772]
116. Drummond RA, Collar AL, Swamydas M, Rodriguez CA, Lim JK, Mendez LM, Fink DL, Hsu AP, Zhai B, Karauzum H, et al. (2015). CARD9-Dependent Neutrophil Recruitment Protects against Fungal Invasion of the Central Nervous System. PLoS Pathog 11, e1005293. 10.1371/journal.ppat.1005293. [PubMed: 26679537]
117. Kumar V, Cheng SC, Johnson MD, Smeekens SP, Wojtowicz A, Giamarellos-Bourboulis E, Karjalainen J, Franke L, Withoff S, Plantinga TS, et al. (2014). Immunochip SNP array identifies novel genetic variants conferring susceptibility to candidaemia. Nat Commun 5, 4675. 10.1038/ncomms5675. [PubMed: 25197941]
118. Roschewski M, Lionakis MS, Sharman JP, Roswarski J, Goy A, Monticelli MA, Roshon M, Wrzesinski SH, Desai JV, Zarakas MA, et al. (2020). Inhibition of Bruton tyrosine kinase in patients with severe COVID-19. Sci Immunol 5. 10.1126/sciimmunol.abd0110.
119. Vosa U, Claringbould A, Westra HJ, Bonder MJ, Deelen P, Zeng B, Kirsten H, Saha A, Kreuzhuber R, Yazar S, et al. (2021). Large-scale cis- and trans-eQTL analyses identify thousands of genetic loci and polygenic scores that regulate blood gene expression. Nat Genet 53, 1300–1310. 10.1038/s41588-021-00913-z. [PubMed: 34475573]
120. Robinson JT, Thorvaldsdottir H, Winckler W, Guttman M, Lander ES, Getz G, and Mesirov JP (2011). Integrative genomics viewer. Nat Biotechnol 29, 24–26. 10.1038/nbt.1754. [PubMed: 21221095]
121. Barrett JC, Fry B, Maller J, and Daly MJ (2005). Haploview: analysis and visualization of LD and haplotype maps. Bioinformatics 21, 263–265. 10.1093/bioinformatics/bth457. [PubMed: 15297300]
122. Gabriel SB, Schaffner SF, Nguyen H, Moore JM, Roy J, Blumenstiel B, Higgins J, DeFelice M, Lochner A, Faggart M, et al. (2002). The structure of haplotype blocks in the human genome. Science 296, 2225–2229. 10.1126/science.1069424. [PubMed: 12029063]
123. Langmead B, and Salzberg SL (2012). Fast gapped-read alignment with Bowtie 2. Nat Methods 9, 357–359. 10.1038/nmeth.1923. [PubMed: 22388286]
124. Liao Y, Smyth GK, and Shi W (2019). The R package Rsubread is easier, faster, cheaper and better for alignment and quantification of RNA sequencing reads. Nucleic Acids Res 47, e47. 10.1093/nar/gkz114. [PubMed: 30783653]
125. Robinson MD, McCarthy DJ, and Smyth GK (2010). edgeR: a Bioconductor package for differential expression analysis of digital gene expression data. Bioinformatics 26, 139–140. 10.1093/bioinformatics/btp616. [PubMed: 19910308]

Highlights

- Complement 5a drives phagocyte survival and effector functions for antifungal defense.
- Extrahepatic C5 production by phagocytes contributes to antifungal protection.
- Impaired complement activation correlates with poor outcomes in humans with candidemia
- Transcriptional induction of a complement module is predictive of human candidemia.

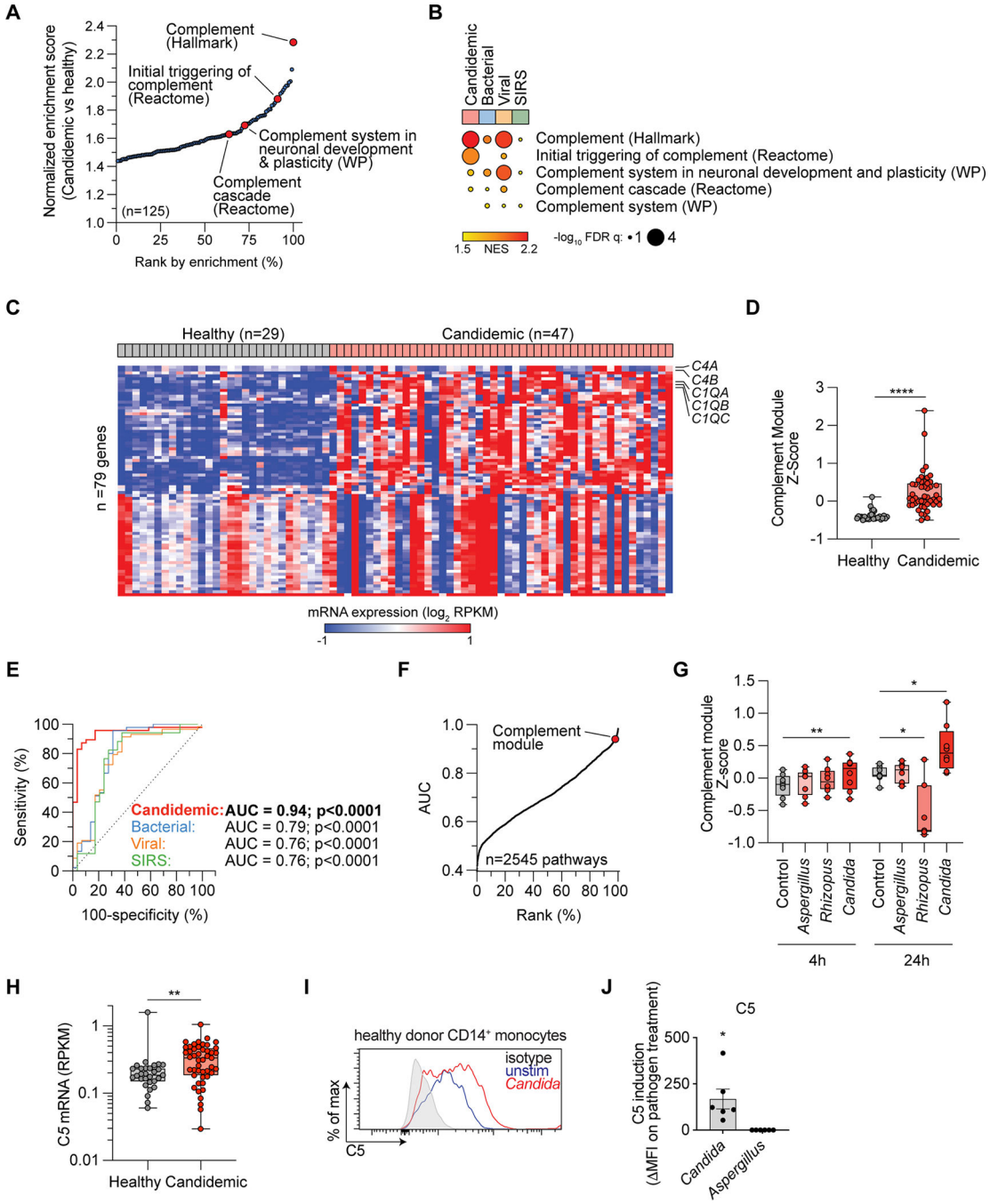

Figure 1. Induced transcription of complement genes in human whole blood is predictive of candidemia. See also Table S1.

(A) Enriched *Hallmark* and *Canonical* MSigDB pathways in blood transcriptomes of candidemic patients compared to healthy controls, ranked by normalized enrichment score (NES). Red denotes complement pathways. Data sourced from GSE176262[17]. **(B)** Dot plot comparing enrichment of complement pathways in patients with candidemia, bacterial or viral infection or systemic inflammatory response syndrome (SIRS) compared to healthy controls. Shown are NES and FDR p-values. **(C)** Heatmap showing the 79-

gene complement module enriched in candidemic patients compared to healthy donors, defined as the leading edge genes of the pathways indicated in red in **A**. Select genes are labeled. **(D)** Mean expression of the complement module in candidemic patients compared to healthy donors. **(E)** Receiver operating characteristic curve showing the performance of the complement module to distinguish candidemic patients, or patients with viral or bacterial infection or SIRS, from healthy donors. Area-under-the-curve (AUC) statistics and P values are shown. **(F)** Plot depicting all 2545 pathways annotated in MSigDB to distinguish candidemic patients from healthy donors, ranked by AUC. Indicated is the position of the complement module identified. **(G)** Mean expression of the complement module in RNA-seq of healthy donor PBMCs challenged *ex vivo* with the indicated fungi. Data sourced from GSE162746[20]. **(H)** Mean expression of *C5* mRNA in whole blood leukocytes in candidemic patients compared to healthy donors. **(I)** Representative FACS histogram showing intracellular C5 protein levels in healthy donor monocytes post-stimulation with heat-killed *Candida*. **(J)** Quantification of intracellular C5 protein in healthy donor monocytes post-stimulation with the indicated fungi (n=6), shown as mean fluorescence intensity difference between stimulated and unstimulated samples. *P<0.05, **P<0.01, ****p<0.0001; unpaired *t*-test **(D)**, one-way ANOVA Brown-Forsythe corrected for multiple comparisons **(G),** Mann-Whitney *U*-test (**H**), Wilcoxon signed-rank test (**J**).

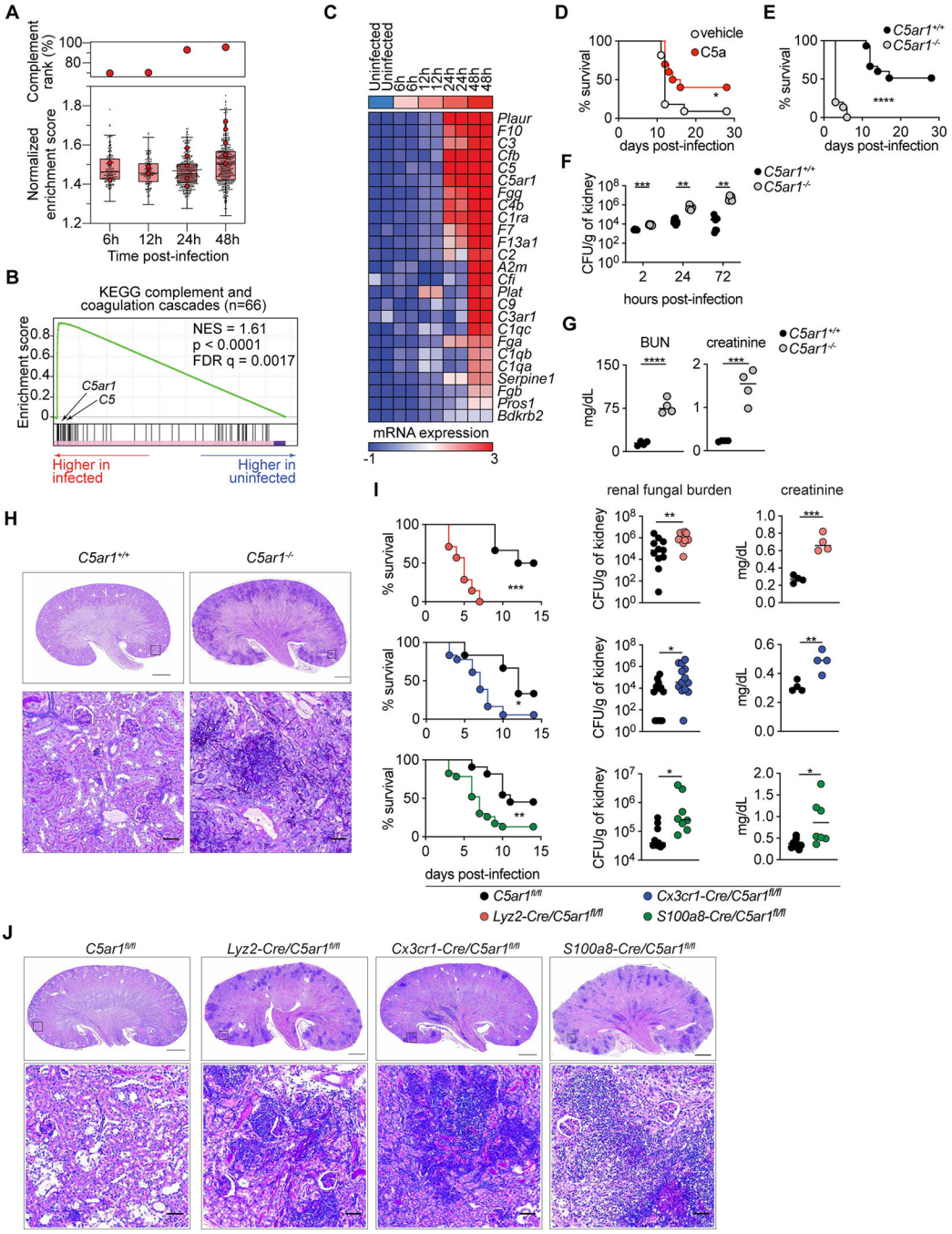

Figure 2. C5a-C5aR1 signaling on phagocytes mediates fungal clearance and host survival during systemic candidiasis. See also Figures S1–S2 and Table S2.

(A) Normalized enrichment scores (NES) for MSigDB pathways enriched in *Candida*-infected kidneys. Red denotes complement pathways. Top panel shows ranks of highest-enriched complement pathways among all pathways. Data sourced from GSE56092[29].

(B) Enrichment plot for the "*KEGG Complement and coagulation cascades*" pathway.

(C) Heatmap showing expression of transcripts, in RPKM, at the leading edge in "**B**".

(D) Survival of vehicle or C5a-treated WT mice post-infection (n=10–11). (**E**) Survival

of WT and *C5ar1*$^{-/-}$ mice post-infection (n=15). **(F)** Renal fungal burden (n=8). **(G)** Serum blood urea nitrogen (BUN) and creatinine (day 3; n=4). **(H)** Histopathology. Representative PAS-stained kidney sections (day 3). **(I-J)** Survival (**I**, left; n=16–32), renal fungal burden (**I**, middle; day 3 for *Lyz2-Cre*^{tg}*C5ar1*$^{fl/fl}$, *Cx3cr1-Cre*^{tg}*C5ar1*$^{fl/fl}$; day 6 for *S100a8-Cre*^{tg}*C5ar1*$^{fl/fl}$; n=8–14), serum creatinine (**I**, right; n=4–7) and renal histopathology **(J)**; representative PAS-stained kidney sections. Scale-bars (for **H,J**): 1 mm (upper), 50 μm (lower). **P*<0.05, ***P*<0.01, ****P*<0.005, *****P*<0.0001; log-rank test (**D-E; I**), 2-way ANOVA with Sidak's multiple comparisons **(F)**, unpaired *t*-test (**G; I**, creatinine), Mann-Whitney *U*-test (**I**, fungal burden).

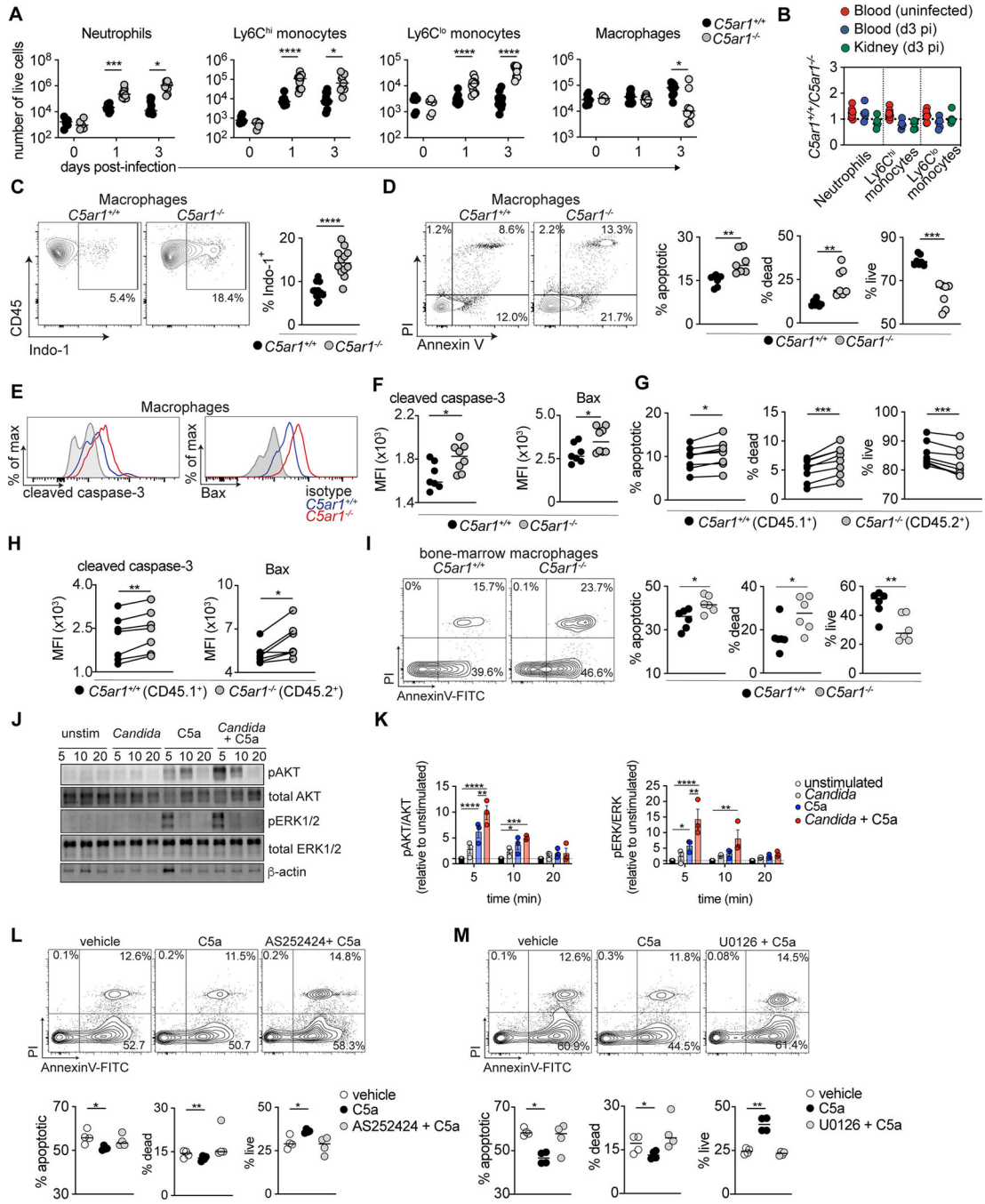

Figure 3. C5aR1 is dispensable for phagocyte trafficking into the kidney but mediates macrophage accumulation and survival. See also Figures S3–S4.

(A) Numbers of renal phagocytes post-infection (n=6–11). **(B)** Relative accumulation of CD45.1$^+$WT and CD45.2$^+$*C5ar1*$^{-/-}$ neutrophils and monocytes in blood and kidneys of mixed BM radiation chimeras (day 3; n=5). **(C-D)** Representative FACS plots (left) and summary data (right) of **(C)** Indo-1$^+$ dead renal macrophages (day 1; n=12), and **(D)** annexin V$^+$PI$^-$ apoptotic, PI$^+$ dead, and annexin V$^-$PI$^-$ viable renal macrophages (day 1; n=7). **(E-F)** Representative histograms **(E)** and mean fluorescence intensity (MFI)

summary data **(F)** for cleaved caspase-3 and Bax in renal macrophages (day 1; n=8). **(G-H)** Summary data of apoptotic, dead, and viable renal macrophages **(G)** and MFI summary data for cleaved caspase-3 and Bax in mixed BM radiation chimeras **(H)** (day 3). (**I**) Representative FACS plots (left) and summary data (right) of apoptotic, dead, and viable BM-derived macrophages after *Candida* co-culture (n=6). (**J-K**) Immunoblot analysis of indicated proteins in WT BM-derived macrophages post-stimulation with indicated stimuli. Representative immunoblot images (**J**) and quantified pixel density values (**K**) are shown. (**L-M**) Representative FACS plots (top) and summary data (bottom) of apoptotic, dead, and viable WT BM-derived macrophages (n=6), following indicated treatments (U0126, ERK1/2 inhibitor; AS252424, PI3K/AKT inhibitor). *P<0.05, **P<0.01, ***P<0.005, ****P<0.0001; Mann-Whitney U-test (**A**, neutrophils and Ly6C^{lo} monocytes at days 1 and 3; Ly6C^{hi} monocytes at day 1; macrophages; **F**, Bax), Welch's t-test (**A**, Ly6C^{hi} monocytes at day 3), unpaired t-test (**F**, cleaved caspase-3; **I**), paired t-test **(G, H)**, 2-way ANOVA with Dunnette's multiple comparisons (**K**), one-way ANOVA with Dunnette's multiple comparisons (**L-M**).

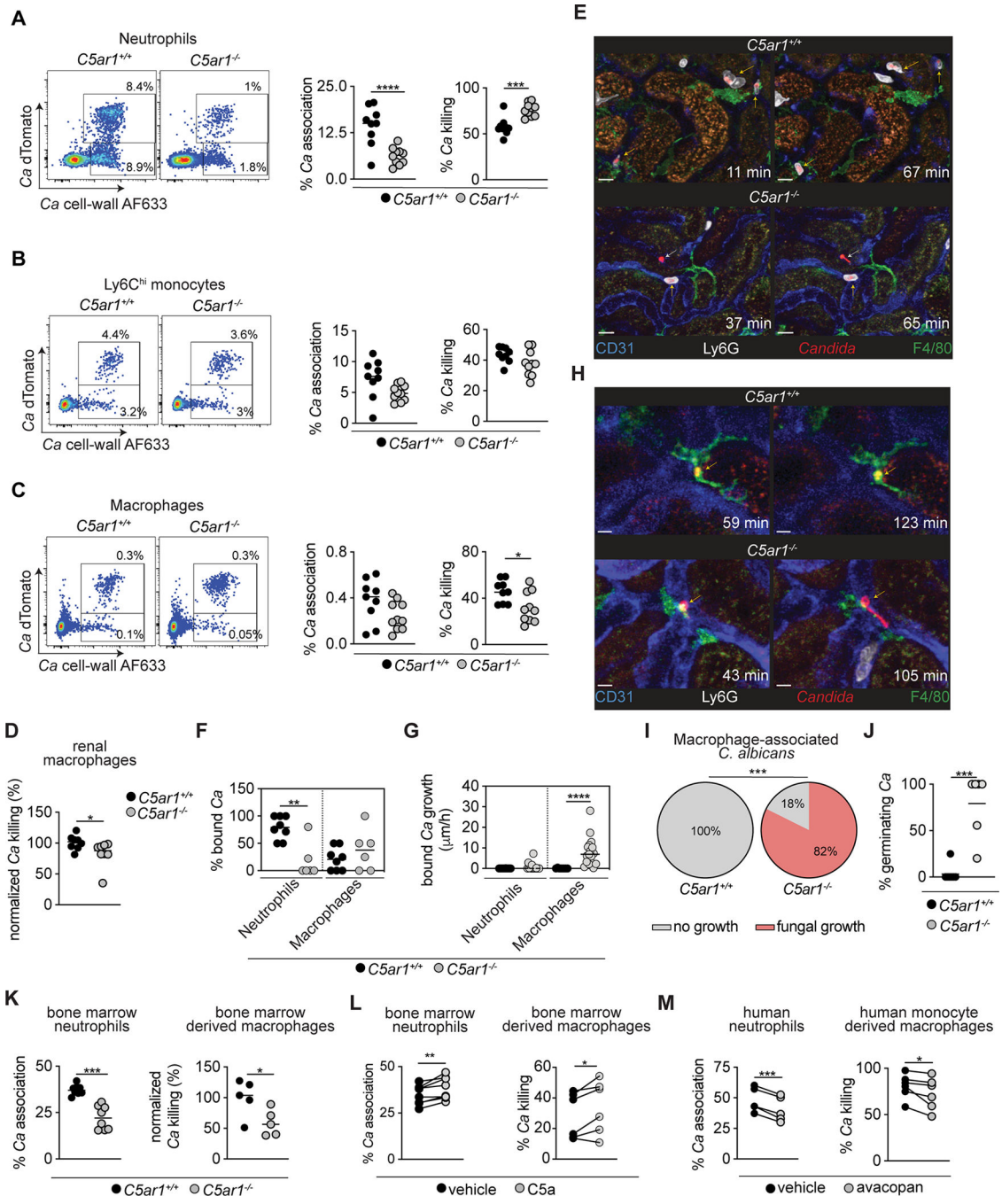

Figure 4. C5aR1 mediates fungal uptake by neutrophils and killing by macrophages. See also Figures S4–S5.

(A-C) Left, representative FACS plots for neutrophils **(A)**, Ly6C^{hi} monocytes **(B)**, and macrophages **(C)** in association with AF633^{+}dTomato^{-} dead or AF633^{+}dTomato^{+} viable *Candida* in WT and *C5ar1*$^{-/-}$ kidneys. Right, summary data of % of cells associating with *Candida* (live+dead *Candida*) and % of dead *Candida* within phagocytes (n=8–10). **(D)** *Candida* killing by FACS-sorted renal macrophages (n=6–8). **(E and H)** Snapshots of kidney intravital imaging at the indicated timepoints post-infection. Yellow arrowheads

mark *Candida* associated with neutrophils/macrophages; White arrowheads mark *Candida* in the *C5ar1*$^{-/-}$ kidney unassociated with neutrophils/macrophages (see also Movie S1). Scale-bars: 50 μm **(E)**, 15 μm **(H)**. **(F)** Pooled data from WT and *C5ar1*$^{-/-}$ mice depicting % of *Candida* stably associated with renal neutrophils/macrophages between 30 and 60 min post-infection (n=6–8). **(G)** Individual fungal cells associated with macrophages (as quantified under "**F**"), were enumerated to indicate whether they exhibited growth or not. **(I)** Growth rate for filamentous hyphae/hour for individual fungal cells associated with neutrophils/macrophages. **(J)** Pooled data from WT and *C5ar1*$^{-/-}$ mice depicting % of *Candida* germinating into hyphae between 30 and 60 min post-infection (n=6–8). **(K-L)** *Candida* uptake by BM neutrophils and killing by BM-derived macrophages (n=6–8). **(M)** *Candida* uptake by human neutrophils and killing by human macrophages (n=5–6). **P*<0.05, ***P*<0.01, ****P*<0.005, *****P*<0.0001; unpaired *t*-test (**A**, %*Ca* killing; **B**; **K**, BM-derived macrophages), Welch's *t*-test (**A**, %*Ca* association; **K**, BM neutrophils), paired *t*-test **(L, M)**, Mann-Whitney *U*-test **(D, J)**, Fisher's exact test **(G)** one-way ANOVA with Tukey's multiple comparisons **(F, I)**.

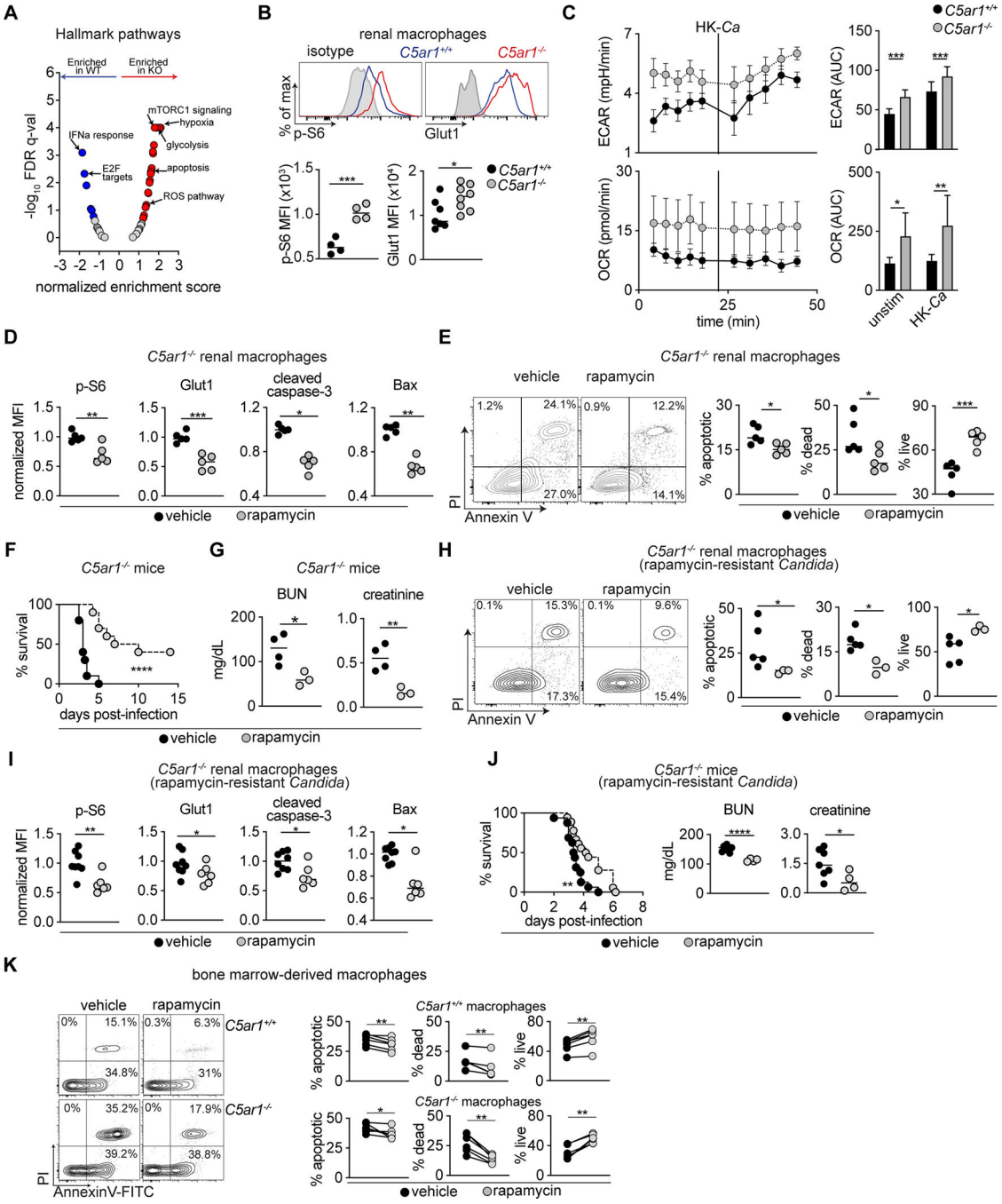

Figure 5. Enhanced mTORC1-associated metabolic rewiring in *C5ar1*$^{-/-}$ macrophages correlates with susceptibility to systemic candidiasis. See also Figure S6 and Table S3.

(A) Enriched MSigDB *Hallmark* pathways, based on GSEA of RNA-seq data from renal macrophages (day 2; n=4/group). **(B)** Representative histograms and mean fluorescence intensity (MFI) summary data for phospho-S6 and Glut1 in renal macrophages (day 2; n=7–8). **(C)** Extracellular flux analysis of renal macrophages (day 1). Left, extracellular acidification rate (ECAR) and oxygen consumption rate (OCR) at baseline and after injection of opsonized heat-killed *Candida* (HK-*Ca*), depicted by the solid line. Right,

area under the curve for ECAR and OCR. Data are pooled from two experiments. **(D-J)** Rapamycin or vehicle were administered in *C5ar1*$^{-/-}$ mice starting at day 1 post-infection. For (**H-J**), mice were infected with the rapamycin-resistant *Candida rbp1Δ/Δ*. **(D, I)** MFI summary data of the indicated proteins in *C5ar1*$^{-/-}$ renal macrophages (day 2). **(E, H)** Representative FACS plots and summary data of annexin V^{+}PI^{-} apoptotic, PI^{+} dead, and annexin V^{-}PI^{-} viable renal macrophages from vehicle or rapamycin-treated *C5ar1*$^{-/-}$ mice (day 2; n=3–5). **(F, J)** Survival of *C5ar1*$^{-/-}$ mice post-infection (n=10). **(G, J)** Serum BUN and creatinine (day 2; n=3–4). **(K)** Representative FACS plots (left) and summary data (right) of apoptotic, dead, and viable BM-derived macrophages after *ex vivo* co-culturing with *Candida rbp1Δ/Δ* (n=6). Quantitative data are means ±SEM. **P*<0.05, ***P*<0.01, ****P*<0.005, *****P*<0.0001; unpaired *t*-test **(B; E; D; G; I; J,** BUN/creatinine**)**, 2-way ANOVA with Bonferroni's' multiple comparisons **(C),** log-rank test **(F; J)**.

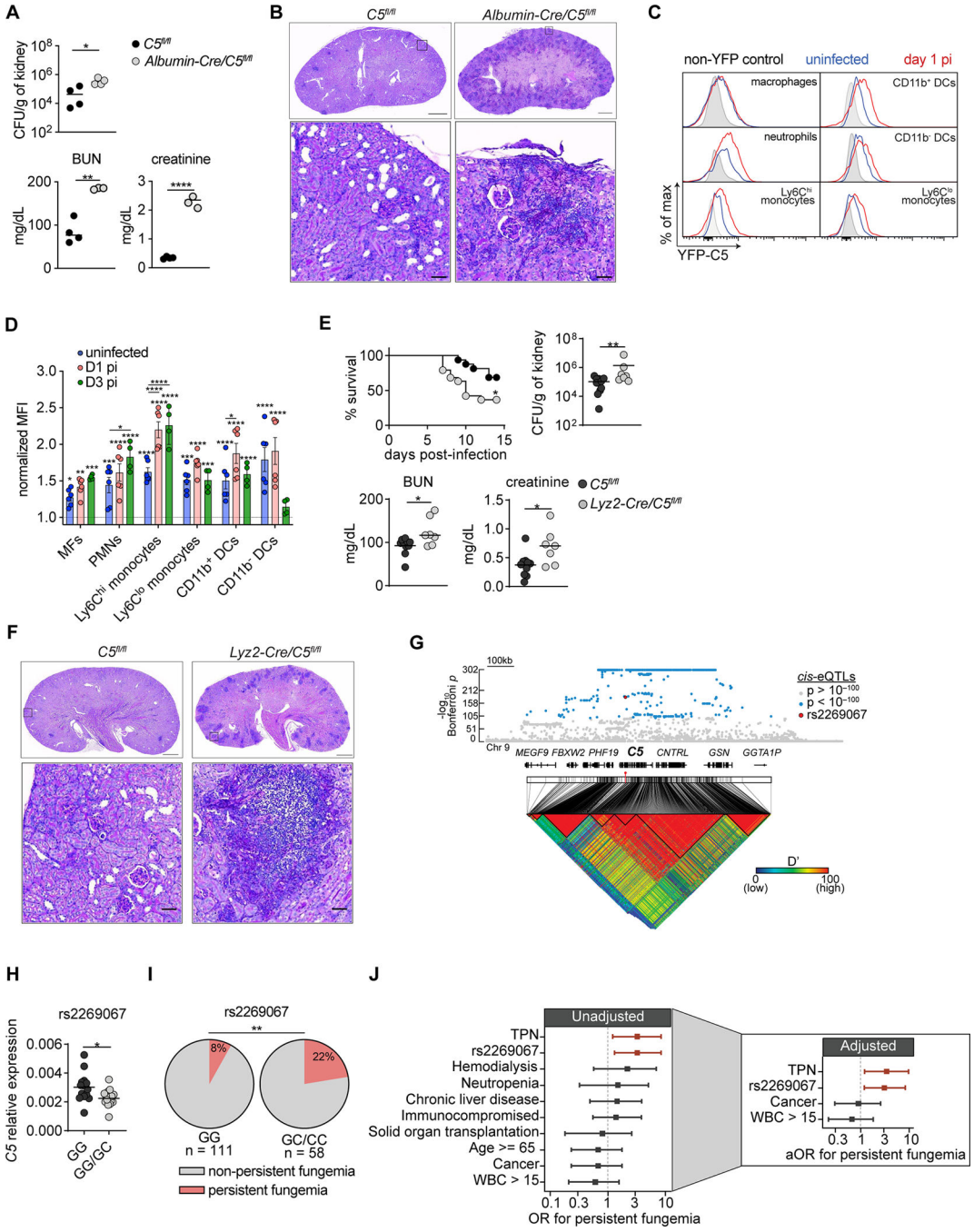

Figure 6: Local C5 production by phagocytes is critical for renal antifungal defense. See also Figure S6.

(A-B) *Albumin-Cre*^{tg}*/C5*$^{fl/fl}$ and *C5*$^{fl/fl}$ mice were evaluated at day 2 post-infection. **(A)** Renal fungal burden, serum BUN and creatinine concentrations (n=3–4). Data are from one of two experiments with similar patterns of results. **(B)** Histopathology. Representative PAS-stained kidney sections. **(C-D)** C5 expression in renal leukocytes. **(C)** Representative FACS. “Red” and “Blue” histograms indicate C5 expression in infected (day 1) and uninfected *YFP-C5*$^{fl/fl}$ reporter mice, respectively; shaded histograms represent infected

non-YFP control mice (n=6–7). **(D)** Summary data of C5-YFP mean fluorescence intensity, normalized to non-YFP controls of each leukocyte subset. **(E-F)** *Lyz2-Cre*^{tg}*/C5*$^{fl/fl}$ and *C5*$^{fl/fl}$ mice were evaluated at day 2 post-infection. **(E)** Survival, renal fungal burden, and serum BUN and creatinine concentrations (n=7–18). **(F)** Histopathology. Representative PAS-stained kidney sections. **(G)** Manhattan plot depicting significant *cis* expression quantitative loci (eQTL). x-axis marks chromosome 9 location, where select genes including *C5* are labeled. y-axis displays $-\log_{10}$ bonferroni *P* values. The dots represent eQTL, blue denotes eQTL with $P<10^{-100}$, and red denotes *C5* SNP rs2269067. The bottom linkage diseqillibrium (LD) plot shows LD analysis of highly-significant eQTL ($P<10^{-100}$) and depicts *C5* SNP rs2269067 to be in strong LD with other top-enriched eQTL affecting *C5* expression. Data sourced from eQTLgen[77]. **(H)** *C5* transcripts in PBMCs of healthy donors with or without *C5* SNP rs2269067. **(I)** Pie chart depicting % of candidemic patients with or without *C5* SNP rs2269067 that exhibited persistent fungemia. **(J)** Forest plots showing odds ratios in univariate and multivariate analyses; horizontal bars, 95% CI. Scale-bars (for **B,F**): 1 mm (upper), 50 μm (lower). Quantitative data are means ±SEM. *$P<0.05$, **$P<0.01$, ***$P<0.005$, ****$P<0.0001$; unpaired *t*-test (**A**, BUN/creatinine; **E**, creatinine), Mann-Whitney *U*-test (**A,E**, fungal burden; **E**, BUN; **H**), 2-way ANOVA with Holm-Sidak's multiple comparisons (**D**), Fisher's exact test (**I**).

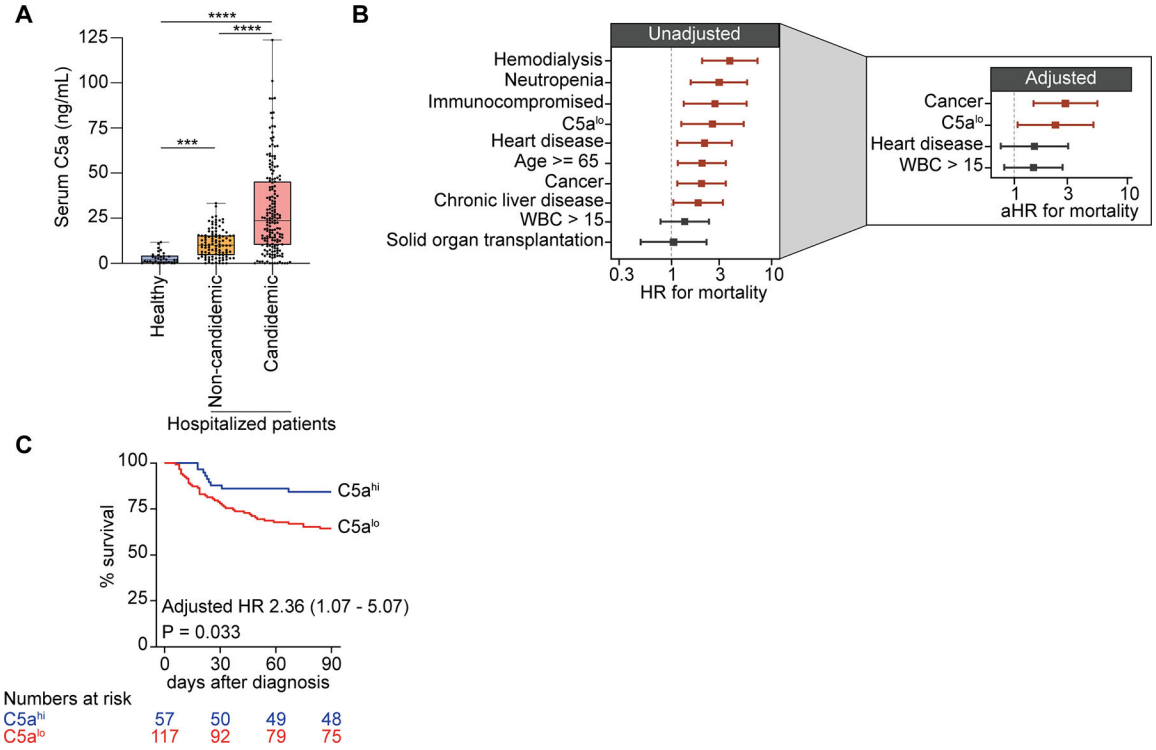

Figure 7. Lower serum C5a concentrations independently correlate with mortality in candidemic patients. See also Tables S4–S7.

(A) Serum C5a concentrations from healthy donors (n=33), candidemic patients (n=174), and non-candidemic hospitalized patients (n=103). **(B)** Forest plots showing hazard ratios in univariate and multivariate analyses; horizontal bars, 95% CI. **(C)** Survival of candidemic patients with $C5a^{lo}$ (<34.7 ng/mL) or $C5a^{hi}$ (≥34.7 ng/mL) status. ****P<0.0001; Kruskal-Wallis test with Dunn's test for multiple comparisons **(A)**, Log-rank test **(C)**.

KEY RESOURCES TABLE

REAGENT or RESOURCE	SOURCE	IDENTIFIER
Antibodies		
rat anti-mouse CD16/CD32	BD Biosciences	Cat#553142, RRID:AB_394657
Brilliant Violet 605™ anti-mouse CD45 Antibody	Biolegend	Cat# 103155, RRID:AB_2650656
PerCP/Cyanine5.5 anti-mouse Ly-6G Antibody	Biolegend	Cat# 127616, RRID:AB_1877271
APC/Cyanine7 anti-mouse/human CD11b Antibody	Biolegend	Cat# 101226, RRID:AB_830642
CD11c Monoclonal Antibody (N418), APC, eBioscience™	Thermo Fisher Scientific	Cat# 17-0114-82, RRID:AB_469346
Alexa Fluor® 700 Rat Anti-Mouse Ly-6C	BD Biosciences	Cat# 561237, RRID:AB_10612017
Biotin anti-mouse CD103 Antibody	Biolegend	Cat# 121404, RRID:AB_535947
MHC Class II (I-A/I-E) Monoclonal Antibody (M5/114.15.2), eFluor™ 450, eBioscience™	Thermo Fisher Scientific	Cat# 48-5321-82, RRID:AB_1272204
PE/Cyanine7 anti-mouse F4/80 Antibody	Biolegend	Cat# 123114, RRID:AB_893478
PerCP/Cyanine5.5 anti-mouse CD3ε Antibody	Biolegend	Cat# 100328, RRID:AB_893318
PerCP/Cyanine5.5 anti-mouse CD19 Antibody	Biolegend	Cat# 152406, RRID:AB_2629815
PerCP/Cyanine5.5 anti-mouse CD335 (NKp46) Antibody	Biolegend	Cat# 137610, RRID:AB_10641137
Bax (D3R2M) Rabbit mAb	Cell Signaling Technology	Cat# 14796, RRID:AB_2716251
Cleaved Caspase-3 (Asp175) Antibody	Cell Signaling Technology	Cat# 9661, RRID:AB_2341188
Recombinant Anti-MLKL (phospho S345) antibody [EPR9515(2)]	Abcam	Cat# ab196436, RRID:AB_2687465
Recombinant Anti-Glutathione Peroxidase 4 antibody [EPNCIR144]	Abcam	Cat# ab125066, RRID:AB_10973901
Phospho-S6 Ribosomal Protein (Ser240/244) (D68F8)	Cell Signaling Technology	Cat# 5364, RRID:AB_10694233
Recombinant Anti-Glucose Transporter GLUT1 antibody [EPR3915]	Abcam	Cat# ab115730, RRID:AB_10903230
Rabbit IgG Isotype Control	Thermo Fisher Scientific	Cat# 02-6102, RRID:AB_2532938
FITC anti-mouse Dectin-1 antibody (2A11)	Bio-Rad	Cat# MCA2289F, RRID:AB_324908
APC anti-mouse CD64 (FcγRI) Antibody	Biolegend	Cat# 139306, RRID:AB_11219391
CD15 Monoclonal Antibody (MMA), eFluor™ 450, eBioscience™	Thermo Fisher Scientific	Cat# 48-0158-42, AB_1907348
Chemicals, Peptides, and Recombinant Proteins		
Corning® 100 mL Penicillin-Streptomycin Solution, 100x	Corning	Cat# 30-002CI
Recombinant Mouse Complement Component C5a Protein	R&D Systems	Cat# 2150-C5-025/CF
Recombinant Mouse Complement Component C3a Protein, CF	R&D Systems	Cat# 8085-C3-025
Animal-Free Recombinant Murine M-CSF	Peprotech	Cat# AF-315-02
Animal-Free Recombinant Human M-CSF	Peprotech	Cat# AF-315-02
Liberase™ TL Research Grade	Millipore Sigma	Cat# 5401020001
DNase I	Millipore Sigma	Cat# 10104159001
EDTA (0.5 M), pH 8.0	Quality Biologicals	Cat# 351-027-101
HEPES Buffer (1 M), pH 7.3	Quality Biologicals	Cat# 118-089-721
ACK Lysing Buffer	Quality Biologicals	Cat# 118-156-721

REAGENT or RESOURCE	SOURCE	IDENTIFIER
Fetal Bovine Serum - Premium, Heat Inactivated	R&D Systems	Cat# S11150H
Corning® RPMI 1640	Corning	Cat# 10-041-CV
Dihydrorhodamine 123	Thermo Fisher Scientific	Cat# D23806
Zymosan	InvivoGen	Cat# tlrl-zyn
PMA	InvivoGen	Cat# tlrl-pma
alamarBlue™ Cell Viability Reagent	Thermo Fisher Scientific	Cat# DAL1100
Triton-X-100	Thermo Fisher Scientific	Cat# A16046.AE
Avacopan	MedChem Express	Cat# HY-17627
Rapamycin	MedChem Express	Cat# HY-10219
AS-252424	Fisher Scientific	Cat# 36-711-0R
U-0126	Fisher Scientific	Cat# 50-197-6090
β-Estradiol	Millipore Sigma	Cat# E8875
Lymphocyte Separation Medium, 1.077g/mL	Lonza	Cat# 17-829E
Ficoll-Paque PLUS	Cytiva	Cat# 17144003
Percoll	Cytiva	Cat# 17089101
SepMate™-50 (IVD)	STEMCELL Technologies	Cat# 85460
Dextran 500	Crescent Chemical Company	Cat# SE18696.01
Polyethylene glycol 400	Sigma Aldrich	Cat# PX1286B-2
TWEEN® 20	Sigma Aldrich	Cat# P7949
TRIzol™ Reagent	Thermo Fisher Scientific	Cat# 15596026
Paraformaldehyde, 4% in PBS	Thermo Fisher Scientific	Cat# J61899.AK
Biotin-XX-SSE	Thermo Fisher Scientific	Cat# B-6352
streptavidin conjugated to Alexa Fluor 633	Thermo Fisher Scientific	Cat# S21375
FCCP	Fisher Scientific	Cat# 04-531-0
Oligomycin	Fisher Scientific	Cat# AAJ61898MA
TWEEN® 20	Sigma Aldrich	Cat# P1379
cOmplete™, EDTA-free Protease Inhibitor Cocktail	Millipore Sigma	Cat# COEDTAF-RO
Halt™ Protease and Phosphatase Inhibitor Cocktail (100X)	Thermo Fisher Scientific	Cat# 78442
eBioscience™ Lipopolysaccharide (LPS) Solution (500X)	Thermo Fisher Scientific	Cat# 00-4976-03
Critical Commercial Assays		
QuantiChrom™ Urea Assay Kit	BioAssay Systems	Cat# DIUR-100
QuantiChrom™ Creatinine Assay Kit	BioAssay Systems	Cat# DICT-500
Anti-Ly6G MicroBeads Ultrapure	Miltenyi Biotec	Cat# 130-120-337
LIVE/DEAD™ Fixable Blue Dead Cell Stain Kit, for UV excitation	Thermo Fisher Scientific	Cat# L34962
eBioscience™ Annexin V Apoptosis Detection Kit	Thermo Fisher Scientific	Cat# BMS500FI-300
RNA Clean-Up and Concentration Kit	Norgen Biotek Corp	Cat# 61000
SMART-Seq v4 full-length transcriptome analysis with ultimate sensitivity for ultra-low RNA input	TaKaRa	Cat# 634894

REAGENT or RESOURCE	SOURCE	IDENTIFIER
Nextera XT DNA Library Preparation Kit	Illumina	Cat# FC-131-1024
Amplex™ Red Hydrogen Peroxide/Peroxidase Assay Kit	Thermo Fisher Scientific	Cat# A22188
Seahorse XF assay medium pack, pH7.4 and calibrant solution	Agilent	Cat# 103680-100, 100840-000
Seahorse XFe96 FluxPak	Agilent	Cat# 102416-100
Human Complement Component C5a DuoSet ELISA kit	R&D Systems	Cat# DY2037
Mouse Complement Component C5a DuoSet ELISA kit	R&D Systems	Cat# DY2150
RNeasy mini kit	QIAGEN	Cat# NA
qScript cDNA Synthesis Kit	Quanta bio	Cat# 95047-100
PerfeCTa® SYBR® Green FastMix®	Quanta bio	Cat# 95074-05K
Perfecta qPCR FastMix UNG Low-ROX	Quanta bio	Cat# 95078-05K
Quick Start™ Bradford Protein Assay Kit 2	Bio-Rad	Cat# 500-0202
Trans-Blot Turbo RTA Mini 0.2 μm PVDF Transfer Kit	Bio-Rad	Cat# 1704272
Radiance Plus ECL substrate	Azure Biosystems	Cat# AC2103
SuperSignal™ West Atto Ultimate Sensitivity Substrate	Thermo Fisher Scientific	Cat# A38555
TaqMan SNP genotyping assay	Thermo Fisher Scientific	Cat# C 2783678_1_
Human C5 specific primers/probe	Thermo Fisher Scientific	Cat# Hs01004342_m1
Human GAPDH specific primers/probe	Thermo Fisher Scientific	Cat# Hs02786624_g1
Deposited Data		
RNA-Seq of kidney macrophages and neutrophils after infection	Current work	Data are deposited at the NCBI's gene expression omnibus (GEO), under accession number GSE206205
Whole blood transcriptome data of healthy volunteers and patients with candidemia, SIRS, or systemic bacterial, and viral infections	Steinbrink et. al.[17]	Deposited data were sourced from the GEO database; accession number GSE176262
Transcriptomes of human PBMC after *ex vivo* stimulation with different fungi	Bruno et. al.[20]	Deposited data were sourced from the GEO database; accession number GSE162746
Murine kidney RNA-Seq data, before and after infection	Liu et. al.[29]	Deposited data were sourced from the GEO database; accession number GSE56092
Experimental Models: Organisms/Strains		
Mouse: CByJ.SJL(B6)-*Ptprc^{a}*/J	Jackson Laboratory	Stock# 006584
Mouse: Balb/cJ	Jackson Laboratory	Stock# 000651
Mouse: C.129S4(B6)- *C5ar1^{tm1Cge}*/J	Jackson Laboratory	Stock# 006845
Mouse: B6.129S4-*C3^{tm1Crr}*/J	Jackson Laboratory	Stock# 029661
Mouse: C57BL/6J	Jackson Laboratory	Stock# 000664
Mouse: B6J.B6N(Cg)- *Cx3cr1tm1.1(cre)Jung/J*	Jackson Laboratory	Stock# 025524
Mouse: *C5ar2$^{-/-}$*	Laboratory of C. Kemper; Gerard et. al.[108]	N/A
Mouse: *YFP-C5$^{fl/fl}$*	Laboratory of C. Kemper; Niyonzima et. al.[15]	N/A
Mouse: *tdTomato-C3$^{fl/fl}$*	Laboratory of C. Kemper; Kolev et. al.[109]	N/A
Mouse: *Albumin-Cre^{tg}/C5$^{fl/fl}$*	Laboratory of C. Kemper	N/A
Mouse: *Lyz2-Cre^{tg}/C5$^{fl/fl}$*	Laboratory of C. Kemper	N/A

REAGENT or RESOURCE	SOURCE	IDENTIFIER
Mouse: *Lyz2-Cre^{ig}/C3$^{fl/fl}$*	Laboratory of C. Kemper	N/A
Mouse: *GFP-C5ar1$^{fl/fl}$*	Laboratory of J. Köhl; Karsten et. al.[31]	N/A
Mouse: *Lyz2-Cre^{ig}/C5ar1$^{fl/fl}$*	Laboratory of J. Köhl; Karsten et. al. [31]	N/A
Mouse: *S100a8-Cre^{ig}*	Laboratory of R. Caspi	N/A
Candida albicans: SC5314	Laboratory of M. Lionakis; Lionakis et. al.[46]	N/A
Candida albicans: CAF2-1-dTomato	Laboratory of M. Lionakis; Lionakis et. al.[46]	N/A
Candida albicans: rapamycin-resistant *rbp1Δ/Δ* strain	Laboratory of J. Heitman; Cruz et. al.[74]	N/A
Oligonucleotides		
Primer: *C5ar1* qPCR; *C5ar1*-F 5' - CAAGACGCTCAAAGTGGTGA - 3'	IDT	N/A
Primer: *C5ar1* qPCR; *C5ar1*-R 5' - TATGATGCTGGGGAGAGACC - 3'	IDT	N/A
Primer: *C5ar2* qPCR; *C5ar2*-F 5' - CTACCGTAGGCTGCTTCAGG - 3'	IDT	N/A
Primer: *C5ar2* qPCR; *C5ar2*-R 5' - CAAATGAAAAACCCCACCAC - 3'	IDT	N/A
Primer: *Hc* qPCR; *Hc*-F 5' - GTCAAGTACACTGCGACTCTTC - 3'	IDT	N/A
Primer: *Hc* qPCR; *Hc*-R 5' - GGCATTGGTACAGCTCATCT - 3'	IDT	N/A
Primer: *Gapdh* qPCR; *Gapdh*-F 5' - AACTTTGGCATTGTGGAAGG - 3'	IDT	N/A
Primer: *Gapdh* qPCR; *Gapdh*-R 5' - ACACATTGGGGGTAGGAACA - 3'	IDT	N/A
Software and Algorithms		
PRISM v8 or 9	Graphpad Software	https://www.graphpad.com/scientific-software/prism/
FlowJo v9 or 10	BD	https://www.flowjo.com/
Imaris v9.2	Oxford Instruments	https://imaris.oxinst.com/
Fiji	NIH[115]	https://imagej.net/software/fiji/
Bowtie 2	Langmead et. al.[123]	https://github.com/BenLangmead/bowtie2
Rsubread	Liao et. al.[124]	https://bioconductor.org/packages/release/bioc/html/Rsubread.html
edgeR	Robinson et. al.[125]	https://academic.oup.com/bioinformatics/article/26/1/139/182458
Haploview 4.2	Barrett et. al.[121]	https://www.broadinstitute.org/haploview/haploview
Integrative Genomics Viewer v2.12.2	Robinson et. al.[120]	https://software.broadinstitute.org/software/igv/
STAR v2.5.2	Dobin et. al.[113]	https://github.com/alexdobin/STAR
Limma	Ritchie et. al.[114]	https://bioconductor.org/packages/release/bioc/html/limma.html

REAGENT or RESOURCE	SOURCE	IDENTIFIER
GSEA v4.2.3	Subramanian et. al.[18]	https://www.gsea-msigdb.org/gsea/index.jsp